This is an open access article published under a Creative Commons Non-Commercial No Derivative Works (CC-BY-NC-ND) Attribution License, which permits copying and redistribution of the article, and creation of adaptations, all for non-commercial purposes.

ACS AUTHORCHOICE

ACS Sustainable Chemistry & Engineering

pubs.acs.org/journal/ascecg

Research Article

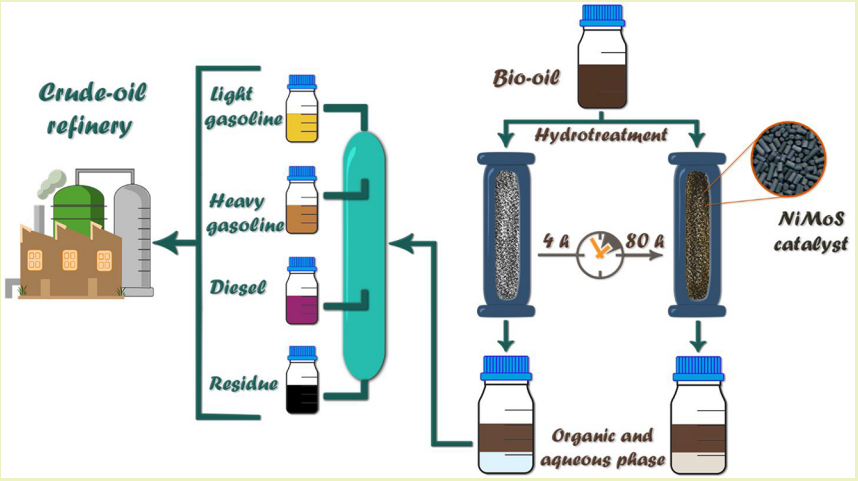
Efficient One-Stage Bio-Oil Upgrading over Sulfided Catalysts

Bogdan Shumeiko,* Miloš Auersvald, Petr Straka, Pavel Šimáček, Dan Vrtiška, and David Kubička

Cite This: *ACS Sustainable Chem. Eng.* 2020, 8, 15149−15167

Read Online

ACCESS | Metrics & More | Article Recommendations | Supporting Information



ABSTRACT: Efficient upgrading of fast pyrolysis bio-oils into products that can be easily integrated into existing refinery complexes remains to be a challenge particularly from the stability of a catalyst performance point of view. Several NiMo catalysts, mainly alumina-supported, were either prepared or acquired and used in hydrotreating of bio-oil from ablative fast pyrolysis of straw. The experiments were carried out in a fixed-bed reactor at 340 °C and 4 MPa and lasted for 80 h. Detailed monitoring of the key physicochemical properties allowed comparing the performance of the catalysts and assessing its changes with the time-on-stream (TOS). The quality of all products deteriorated with the increasing TOS evidencing gradual loss of performance. Nonetheless, the product quality over the best catalysts remained suitable for further refinery upgrading by coprocessing during the 80-h TOS. Distillation of a hydrotreated bio-oil into naphtha, gas oil, and atmospheric residue allowed obtaining further insights into oxygenates present and their distribution.

KEYWORDS: *Bio-oil upgrading, Hydrotreatment, Sulfided catalysts, Long-term stability, Distillation*

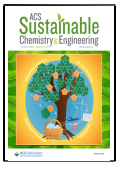
INTRODUCTION

Lignocellulosic biomass-based liquid biofuels have attracted much attention as a potential sustainable liquid hydrocarbon fuel source. Fast pyrolysis has been considered to be the most suitable lignocellulosic biomass conversion technology because it produces the highest yield of bio-oil, i.e., liquid organic products.[1−3] Apart from bio-oil (yield 40−70 wt %), the pyrolysis process affords also gaseous products (10−20 wt %) and char (15−40 wt %). The bio-oil has typically high oxygen content due to the presence of alcohols, phenols, ketones, aldehydes, furans, acids, and water.[4] Consequently, bio-oils have a low heating value and high acidity, corrosivity, and water content and must be thus upgraded before their use as engine fuels.[5,6]

Technologies proposed to upgrade bio-oils include catalytic cracking, steam reforming, and hydrotreatment.[5] The latter seems to be the most effective as it leads to the highest yields of a potentially petroleum-refinery-compatible feedstock.[5,7,8] In addition, hydrotreatment is a well-established technology for the upgrading of crude-oil distillates, and thus, the coprocessing of stabilized bio-oils with crude-oil distillates could be used to reduce the cost of bio-oil upgrading.

Thus far, bio-oil hydrotreatment has been studied over various catalysts; namely, those based on reduced noble (Pd, Pt, Ru) or transition (Ni, Fe, Cu, Co, Mo) metals or on sulfided metals (Ni−Mo, Co−Mo, Ni−W) supported over various carriers (Al_2O_3, SiO_2, TiO_2, C).[7,9−15] Each type of these catalysts has its advantages and disadvantages. Noble metal catalysts have shown the highest hydrogenation activity,

Received: May 26, 2020
Revised: September 11, 2020
Published: September 28, 2020



Downloaded from pubs.acs.org/ascecg/article-pdf/8/40/15149/6712170/acssuschemeng.0c03896.pdf by UNIV CHEMISTRY & TECHNOLOGY PRAGUE user on 26 October 2026

© 2020 American Chemical Society

but their high cost and facile poisoning by even low amounts of sulfur or nitrogen make them less favorable for feedstocks containing already small amounts of heteroatoms and other impurities, as most bio-oils do.[10] Transition metals are cheaper and more robust, and even their poisoned sulfide form ($Ni_{catalyst}$ + $S_{feedstock}$ = $NiS_{catalyst}$) possesses a slight hydrogenation activity; but they are dramatically lower than that of reduced metals.[16]

Compared with noble and transition metals, metal sulfide catalysts have higher resistance to sulfur poisoning, and their robustness proven in industrial upgrading of even heavy petroleum fractions makes them good candidates for bio-oil upgrading due to them. High catalytic activity is obtained by sulfiding supported bimetallic phases, such as NiMo, due to a synergy effect as the hydrotreating activity of sulfided NiMo exceeds that of sulfided Ni or Mo. The activity of sulfided catalysts is typically maintained by sulfur compounds in the feedstock that yield H_2S. As bio-oils are low-sulfur feedstocks in comparison with crude-oil fractions, adding extra sulfur to the bio-oils is necessary to maintain the sulfided catalysts in their active form.[17−19] Despite their robustness, the crucial issue with sulfided catalysts, as with the other types, is their stability during the long-term bio-oil hydrotreatment.

The hydrotreatment of bio-oil over sulfided catalysts has been investigated for various feedstocks under a wide range of reaction conditions (T = 200−450 °C, p = 1−29 MPa),[7,11,17,20−23] in batch and fixed-bed reactors. The advantage of a batch reactor is its simplicity compared to a fixed-bed reactor allowing fast screening and comparison of catalytic activity of different catalysts. French et al. tested various Pd, Ru, and $NiMoS/Al_2O_3$ catalysts at the different reaction conditions (T = 150−400 °C and pressure 40−160 bar).[24] It was possible to obtain as good performance with a sulfided NiMo catalyst as with a Pd catalyst and even a better reduction in bio-oil acidity. Ardiyanti et al.[25] performed a series of hydrogenation experiments of wood-based pyrolysis oil over Rh-, Pd-, and Pt-supported catalysts and a $CoMo/Al_2O_3$ catalyst at 350 °C, 200 bar, and a 4-h reaction time. Noble catalysts showed good results in bio-oil upgrading; however, $CoMo/Al_2O_3$ also performed well and showed an even higher H/C ratio and a lower moisture content in upgraded bio-oil. Bio-oil hydrodeoxygenation as well as upgrading of bio-oil model compounds have been extensively reviewed,[26−28] and specific studies of model compounds such as aromatics, anisole, guaiacol, phenol, and other oxygenates have been reported.[29−33] Hydrogenation of model compounds can give a good overview of the selectivity of the catalysts to the specific reaction pathways; however, it does not afford enough information on the competitive reactions of the different compounds present in bio-oils. For example, Viljava et al.[34] reported that with an additional sulfiding agent in a form of H_2S (for sulfided NiMo and CoMo catalysts) the conversion and hydrodeoxygenation of phenol were suppressed; but for anisole, the conversion and demethylation reaction slightly increased in the presence of H_2S. However, Wang et al.[35] reported that adding benzothiophene to p-cresol improved p-cresol conversion and even increased the selectivity to saturated products. Wang et al.[35] stated that the S atom in benzothiophene was removed in the form of H_2S after HDS. These H_2S molecules were adsorbed on active sites of Co−Mo−S, reduced the negative effect of water on the sulfide structure, and finally inhibited the deactivation of the catalyst, which resulted in the higher conversion than that without adding benzothiophene; but excessive H_2S occupied more active sites due to a competitive adsorption between H_2S and p-cresol on the Co−Mo−S catalyst and then decreased the available active sites for the HDO reaction. So, many factors should be considered in the hydrogenation of model compounds before the application of this catalyst on the real bio-oil.

Many bio-oil hydrogenation studies were also performed in fixed-bed reactors, but only a few of these studies have been focused on the long-term stability of such catalysts. Routray et al.[36] studied white oak bio-oil hydrogenation over nonsulfided catalysts in a two-zone fixed-bed reactor. The low-temperature zone was filled with a Ru/C catalyst to saturate the most reactive compounds, whereas the high-temperature zone (300−400 °C) was filled with a Pt/zirconium phosphate catalyst to deoxygenate the less reactive compounds. The addition of the second high-temperature catalytic zone allowed producing a hydrocarbon oil similar to petroleum-based fuels. However, coke formation was a problem that led to a decrease in oil yields. A similar problem was reported also by Elliot et al.[20] who studied the long-term hydrotreatment of Finnish pine bio-oil in a two-stage fixed-bed reactor (first stage: Ru/C catalyst at 170 °C; second stage: sulfided Ni−Mo or Co−Mo catalyst at a reaction temperature of 400 °C and pressure of 13.8 MPa). However, the experiment was terminated at the time-on-stream (TOS) of approximately 90 h due to coke formation at the interface of the two catalyst beds and an increase in the pressure drop. As the pressure drop increased, the quality of the hydrotreated products decreased (lower H/C ratio, higher total acid number, higher density), eventually leading to the formation of an emulsion with no observable separation into two phases. Interestingly, compared with the Co−Mo catalyst, the Ni−Mo catalyst yielded products with a higher H/C ratio at the expense of higher hydrogen consumption.[19] In 2011, Pacific Northwest National Laboratory (PNNL) reported that 140 h was the longest possible hydrotreatment operation before the plugging of the catalyst bed by coke.[37] Later, PNNL had started to use a low-temperature pretreatment reactor with the Ru/C catalyst that slightly decreased product density and enabled the extension of the operation time up to 1440 h.[23] However, plugging of the first reaction zone occurred at the TOS of 750 h, and after replacement of the catalyst in this reaction zone, the experiment continued for a further 690 h. Despite these advances, up to date, the only long-term stability studies of hydrotreatment of bio-oil over sulfided catalysts have involved a two-stage setup with noble metals used in the first reaction zone. This setup makes such hydrotreatment operationally complicated and economically unfavorable.

Here, we present the results of a long-term (80 h) hydrotreatment of wheat/barley (50/50 wt %) straw bio-oil in a one-stage fixed-bed reactor under stable reaction conditions (340 °C; 4 MPa), chosen according to the results of our previous study showing that at these conditions the highest deoxygenation, low hydrogenation of aromatic rings and lower hydrotreatment operational costs could be achieved.[7] We compare the long-term activity of various lab-made and commercial sulfided Ni−Mo catalysts based on their physicochemical properties (density, viscosity, elemental analysis, etc.) and on the chemical composition of the hydrotreated products. The objective was not to fully deoxygenate the bio-oil but to prepare a feedstock compatible with the petroleum refinery fraction, i.e., a product suitable for

Downloaded from pubs.acs.org/ascecg/article-pdf/8/40/15149/6712707/acssuschemeng.0c03896.pdf by UNIV CHEMISTRY & TECHNOLOGY PRAGUE user on 26 October 2026

https://dx.doi.org/10.1021/acssuschemeng.0c03896
ACS Sustainable Chem. Eng. 2020, 8, 15149−15167

Table 1. Catalysts and Experiment Description

expt	target composition	preparation	particle sieved size [mm]	bulk density [g·L^{-1}]
Exp_1/C	commercial Ni−Mo/Al_2O_3		0.84−1.2	500
Exp_2/C	commercial Ni−Mo/Al_2O_3		0.84−1.0	1000
Exp_3/L	lab-made Ni(3.9%)Mo(15%)/Al_2O_3	two-step impregnation with calcination	0.84−1.0	820
Exp_4/L	lab-made Ni(3.9%)Mo(15%)/Al_2O_3	coimpregnation	0.84−1.0	820
Exp_5/L	lab-made Ni(3.9%)Mo(15%)/SiO_2	two-step impregnation	0.8−1.2	588
Exp_6/L	lab-made Ni(3.9%)Mo(15%)/Al_2O_3	two-step impregnation with drying	0.84−1.0	820

Table 2. Selected Catalysts Properties

				composition [wt %]				
name	BET surface [m^2·g^{-1}]	pore volume [cm^3·g^{-1}]	MV[c] [cm^3·g^{-1}]	Ni	Mo	Al_2O_3	SiO_2	Ni/Mo a.r.[b]
alumina	135.5	0.552	0.0025			100		
Exp_1/C	163.2	0.650	0.0086	1.71	6.62	87.76		0.42
Exp_2/C	*a*	*a*	*a*	*a*	*a*	*a*	*a*	*a*
Exp_3/L	78.9	0.317	0.0034	3.05	15.22	76.14		0.33
Exp_4/L	86.5	0.369	0.0037	2.45	13.36	75.12		0.30
Exp_5/L	94.6	0.531	0.0066	3.01	16.82		70.43	0.29
Exp_6/L	79.5	0.343	0.0036	3.20	14.71	68.22		0.38

[a]Not measured in accordance with the terms of the catalyst provision. [b]Atomic ratio, elemental composition determined by ICP-MS except Exp_1/C that was measured by XRF. [c]Micropore volume.

coprocessing in a petroleum refinery. A quick assessment of the "catalyst health" based on its performance is important to optimize the operation parameters during an experiment. Thus, we have combined FTIR of collected products at a certain time-on-stream with principal component analysis (PCA) to take a snapshot of the catalyst health and product quality at various times-on-stream during long-term experiments.

MATERIALS AND METHODS

Feedstock. The bio-oil was obtained from fast pyrolysis of wheat/barley straw (50/50 wt %) in an ablative reactor at a temperature of 550 °C and vapor residence time of less than 3 s performed at Fraunhofer UMSICHT. Vapors condensed at a temperature of 2−5 °C spontaneously separated into an aqueous and an oily phase. The oily (organic) phase was used as a feedstock in our experiments. The feedstock was doped with 0.5 wt % of dimethyl disulfide (DMDS) to preserve the catalyst in its active, i.e., sulfided form. The detailed physicochemical properties of the used bio-oil were presented previously.[7]

Hydrotreatment Experiments. A fixed-bed reactor (stainless steel, L: 320 mm, d: 23 mm) with a cocurrent down flow of feedstock and hydrogen was used for the hydrotreatment experiments. There was a thermowell (outer diameter 4 mm) placed in the reactor axis with 10 thermocouples. The upper half of the catalyst bed was used as a preheating zone with a gradually increasing temperature to the target temperature of 340 °C. The lower half of the catalyst bed was used as the main reaction zone.

Crushed and sieved catalysts were sulfided *in situ* (345 °C, 4 MPa) by hydrotreated gas oil spiked with 3.8 wt % of DMDS. The catalyst activation was followed by 24 h of hydrotreating of a straight-run gas oil (SRGO) containing 0.23 wt % of sulfur to stabilize the catalyst and assess its desulfurization activity. The stabilization was carried out at a temperature of 340 °C, hydrogen pressure of 4 MPa, and LHSV of 0.5 h^{-1}. The description of laboratory-made catalyst preparation is presented in the Supporting Information in the section Catalyst Preparation and Characterization (pages S-2 and S-3), and the scheme of lab-made catalyst preparation is presented in Figure S1.

Bio-oil was hydrotreated at a temperature of 340 °C, H_2 pressure of 4 MPa, feedstock flow rate of 50 g·h^{-1} (corresponding to LHSW of 0.5 h^{-1}), and hydrogen to feedstock volume flow rate ratio of 1800:1. The liquid products were collected cumulatively every 4 h, and gaseous products were sampled into Tedlar sampling bags. After bio-oil hydrotreatment, the reactor was flushed, heated, and dried under the flow of hydrogen. The unloaded catalysts were sampled and analyzed by elemental analysis to determine the carbon content according to ASTM D5291-16 described below. The description of liquid and gaseous product characterization is presented in the Supporting Information in section Analysis of Bio-Oil and Products of Hydrotreating (pages S-3−S-5).

RESULTS AND DISCUSSION

Catalyst Properties and HDS Activity. Catalyst composition and basic textural properties are presented in Tables 1 and 2. Since all lab-made alumina-supported catalysts were prepared using the same alumina as a support and the same target loading of the active phase, their textural properties (BET surface, pore volume, and bulk density) did not differ significantly (Table 2). The loading of the active NiMo phase resulted in about a 40% decrease in the total specific surface area (see Table 2). In contrast, the BET area of the commercial catalyst (Exp_1/C) was about twice as high as the BET area of the lab-made alumina catalysts (ca. 80 vs 163 m^2/g). This was also reflected by its almost doubled total pore volume (0.650 vs 0.357 cm^3/g) (Table 2). Consequently, the catalyst used in Exp_1/C had a significantly lower bulk density than the lab-made alumina-based catalysts. So in the same reactor volume, there was a lower amount of the active catalyst. N_2-adsorption−desorption isotherms for the selected catalysts and alumina can be found in the Supporting Information in Figure S2. All isotherms were IV type with an H1 hysteresis loop according to IUPAC.

Pore volume distribution was also different for the commercial alumina-based catalyst (Exp_1/C) and the lab-made one (e.g., Exp_3/L) as a consequence of different alumina used (Figure 1). This can be seen by the difference in the average pore diameter of Exp_1/C catalysts and the alumina support that was used to prepare catalysts Exp_3/L, 4/L, and 6/L. The lab-made catalyst Exp_3/L (also 4/L and 6/L) had an average pore diameter of 16 nm similar to alumina. The commercial catalyst Exp_1/C showed a smaller average pore diameter of about 11 nm. Different behavior

https://dx.doi.org/10.1021/acssuschemeng.0c03896
ACS Sustainable Chem. Eng. 2020, 8, 15149−15167

Downloaded from pubs.acs.org/ascecg/article-pdf/8/40/15149/6712707/acssuschemeng.0c03896.pdf by UNIV CHEMISTRY & TECHNOLOGY PRAGUE user on 26 October 2026

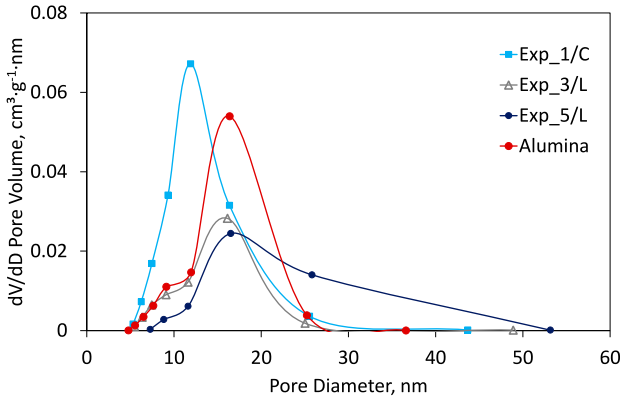


Figure 1. Pore size distribution for the commercial catalyst Exp_1/C, alumina used for lab-made catalysts, the alumina-based catalyst Exp_3/L, and the silica-based catalyst Exp_5/L.

showed the silica-based catalyst Exp_5/L, where its BJH desorption distribution curve had a broad peak showing the presence of pores in the range approximately from 8 to about 35−40 nm (Figure 2).

Although the lab-made alumina-supported catalysts had close elemental composition and textural properties (Table 2), their HDS activity during the catalyst stabilization step (Table 3) differed significantly, which can be also explained by different Ni/Mo atomic ratios (Table 2). It should be mentioned that the coimpregnated catalyst (Exp_4/L) had the lowest Ni loading and Ni/Mo atomic ratio. While the two-step impregnation procedure with calcination as well as the coimpregnation afforded catalysts with similar HDS activity (sulfur content after stabilization ca. 70 ppm), the catalyst prepared by the two-step procedure, but only with intermediate drying between the impregnation steps, resulted in the least active alumina-supported HDS catalyst (100 ppm of S in product after stabilization). Both commercial catalysts showed a better HDS performance than the lab-made ones. While the HDS performance of the catalyst in Exp_2/C was only slightly better (final S concentration of about 60 ppm), the catalyst in Exp_1/C yielded products with only 12 ppm of S (Table 3). The silica-supported catalyst showed the lowest HDS activity resulting in the sulfur concentration in product samples around 500 ppm.

Products Yields in Bio-Oil Upgrading. The products of bio-oil upgrading by hydrotreating separated spontaneously into two liquid phases—a dark brown organic phase and a clear colorless aqueous phase. When alumina-supported catalysts were used, the organic phase was during the whole course of experiments the lighter phase, i.e., on top of the aqueous phase. In contrast, it was the lower phase, i.e., under the aqueous phase, when the silica-supported catalyst was used. The higher density of the organic phase than that of the aqueous phase can serve as the first indication of the insufficient catalyst deoxygenation activity as suggested by Elliot et al.[20] They hydrotreated bio-oil in a two-stage process (the first stage with Ru/C and the second with $NiMo/Al_2O_3$), and the experiment was stopped after 90 h of TOS because of reduced catalytic activity.[19] The decrease in catalyst activity resulted in a lower product quality due to the hindered separation of the upgraded organic phase from the aqueous one. Ultimately, formation of emulsions was observed.

As the quality of products in the experiment over $NiMo/SiO_2$ (Exp_5/L) was obviously significantly worse than those obtained over alumina-supported catalysts, the temperature and pressure in the experiment Exp_5/L were increased to 360 °C and 8 MPa, respectively, to enhance the product quality. However, despite the increased temperature and pressure, the quality of the products obtained over $NiMo/SiO_2$ remained still visually worse than the quality of products prepared over $NiMo/Al_2O_3$ catalysts at milder conditions. Thus, the experiment was stopped after 36 h on stream to prevent excessive coking of the catalyst bed and potential technical issues during catalyst unloading. The picture of upgraded products is presented in the Supporting Information in Figure S3.

The collected reaction products were then separated into an organic and an aqueous phase. First, the spontaneously separated aqueous phase was removed, and then the organic

Table 3. Sulfur Content (ppm) in the SRGO after HDS

TOS [h]	sulfur amount [mg·kg^{-1}]					
	Exp_1/C	Exp_2/C	Exp_3/L	Exp_4/L	Exp_5/L	Exp_6/L
4	8.7	48	63	13	504	97
8	8.9	51	67	32	512	106
12	9.4	53	65	40	499	112
16	11.5	55	60	53	493	139
20	11.7	58	63	61	493	101
24	11.9	60	70	72	481	104

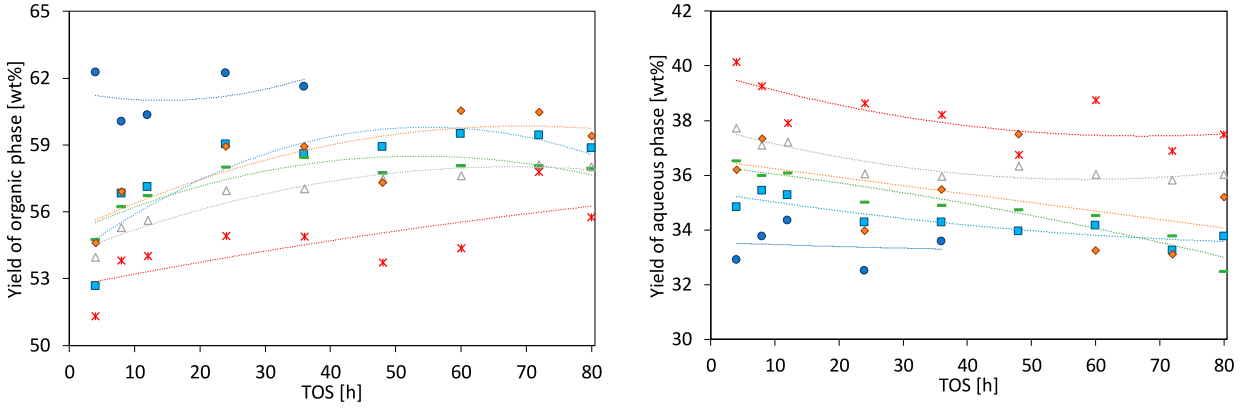


Figure 2. Yields of the organic phase (A) and the aqueous phase (B) of the liquid reaction products. ■ (blue) Exp_1/C, ◊ (orange) Exp_2/C, Δ (gray) Exp_3/L, ∗ (red) Exp_4/L, ● Exp_5/L, − (green) Exp_6/L.

Downloaded from pubs.acs.org/ascecg/article-pdf/8/40/15149/6712707/acssuschemeng.0c03896.pdf by UNIV CHEMISTRY & TECHNOLOGY PRAGUE user on 26 October 2026

https://dx.doi.org/10.1021/acssuschemeng.0c03896
ACS Sustainable Chem. Eng. 2020, 8, 15149−15167

phase was additionally centrifuged to separate all water drops left on the flask walls. The weight yields of organic and aqueous phases relative to the bio-oil fed in the reactor are shown in Figure 2. In line with the observations described above, the products from experiment Exp_5/L ($NiMo/SiO_2$) had the highest yield of the organic phase and, thus, the lowest yield of the aqueous phase (Figure 2). This can be attributed to the lowest bio-oil deoxygenation resulting in the lowest water formation and higher organic phase polarity, thus, more water dissolved in the organic phase.

Among the alumina-supported catalysts, the lab-made catalyst used in the experiment Exp_4/L showed the highest deoxygenation activity and, thus, the highest yield of the aqueous phase over the complete course of the experiment (Figure 2). The yields of the organic phase were for the alumina-supported catalysts in the range 50−60 wt % during the 80-h TOS (Figure 2). Surprisingly, the commercial catalysts, particularly the one used in Exp_1/C, exhibited lower deoxygenation activity, i.e., yielded less water, despite their higher HDS activity discussed above. It can thus be inferred that the HDS activity cannot be used as a measure for predicting deoxygenation activity. As expected, the yield of the organic phase increased with the increasing TOS reflecting the suppressed deoxygenation activity due to the deactivation of the catalysts. The highest deactivation rate was observed until about 40 h of the TOS (Figure 2). After this time, the yields of aqueous and organic phases were stable (Figure 2).

The content of solid particles in raw bio-oil was 0.2 wt %, and bio-oil with this content was successfully refined for 80 h without any obvious pressure drop in the catalytic bed.

Physicochemical Properties of Liquid Products. All obtained liquid products were analyzed in detail by an array of analytical methods to characterize their properties and their changes with the TOS and, thus, to assess rigorously the performance of the different tested catalysts. The overall changes in the chemical composition of the organic phase of the liquid products can be seen from the Van Krevelen diagram (see Figure 3) presenting the H/C vs O/C ratio. The inset picture provides an overview depicting two extremes—i.e., bio-oil as the raw material and diesel as the ultimate target product. When $NiMo/Al_2O_3$ catalysts were used for bio-oil upgrading, the composition of the organic phase products lies roughly on a line connecting the two extremes. This demonstrates that deoxygenation (decrease in O/C ratio) as well as hydrogenation (increase in H/C) took place (Figure 3). On the contrary, the composition of the products obtained over $NiMo/SiO_2$ indicates that only moderate hydrogenation occurred but virtually no deoxygenation (Figure 2). It should be noted that residual water droplets may be present in the sample of the product Exp_5/L that could affect the elemental composition but would not be properly determined as water content (Figure 4C). This can be seen in some samples having a higher O/C ratio than the original bio-oil.

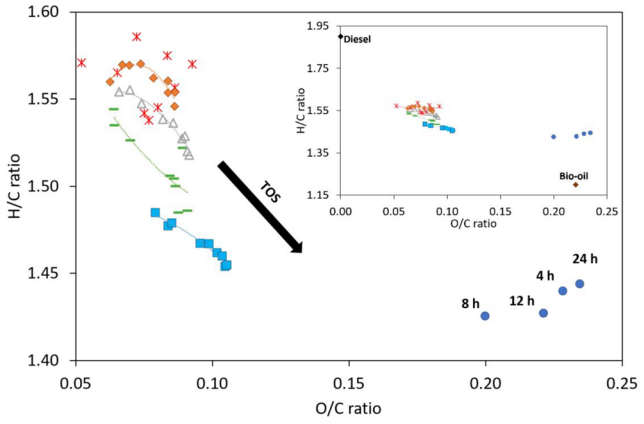


Figure 3. Van Krevelen graph of diesel (♦), feed bio-oil (◊, brown), and hydrogenated products with the zoomed region of the products for detail overview. ■ (blue) Exp_1/C, ◊ (orange) Exp_2/C, Δ (gray) Exp_3/L, ∗ (red) Exp_4/L, ● Exp_5/L, − (green) Exp_6/L.

A closer look at the elemental composition data reveals that both O/C increased while H/C decreased gradually with the increasing time-on-stream (Figure 3). While this trend is pronounced with one of the commercial catalysts (Exp_1/C) and two of the lab-made catalysts (Exp_3/L and Exp_6/L), it is less severe in Exp_2/C and not distinguishable in Exp_4/L (Figure 3). The decrease in the H/C ratio and the increase in the O/C indicate deterioration in the catalyst performance. Thus, it can be concluded that the catalysts used in Exp_2/C and Exp_4/L are the most stable catalysts among the tested ones. Priharto et. al[18] also reported high deoxygenation activity of $NiMo/Al_2O_3$ catalysts in the upgrading of pyrolysis oil from lignin-rich digested stillage under even more severe reaction conditions (350 °C, 10 MPa, and the 4-h TOS) in a batch reactor producing a comparable hydrogenated product to that obtained in Exp_4/L.

The sulfur content in organic liquid products was an important parameter as a sign of catalyst HDS activity. As we mentioned in the Materials and Methods section, we doped raw bio-oil (0.07 wt % S) with 0.5% DMD (0.34 wt % S) for catalytic activity maintenance, so the total sulfur amount for the feedstock was 0.41 wt % dry basis. However, the sulfur content in all hydrogenated organic products was 10−20 times lower than in the feedstock. The poorest HDS activity of the feedstock showed silica-supported catalyst Exp_5/L (0.04 wt % S at the 24-h TOS), all alumina-supported catalysts (lab-made and commercial) performed identically, and the sulfur content for all experiments TOS was at the level of 0.02 wt % (dry basis).

The differences in the catalytic activity and its stability can be also observed on the variation of the physicochemical properties of bio-oil upgrading products with the time-on-stream (see Figure 4). The results unequivocally confirm the much worse performance of the $NiMo/SiO_2$ catalyst in comparison with the $NiMo/Al_2O_3$ catalyst studies (Figure 4). Although the product viscosity, water content, and MCR decreased approximately four times in comparison with the original bio-oil during Exp_5/L, with all tested $NiMo/Al_2O_3$ catalysts the reduction was more significant. As the test Exp_5/L at stable reaction conditions (340 °C and 4 MPa) was only short (24 h) due to the insufficient catalytic performance of the $NiMo/SiO_2$ catalyst, it is impossible to evaluate properly the catalyst stability. Nonetheless, the initial points suggest that the catalyst activity was stable, i.e., there is no significant change in density, viscosity, or water content during the 24-h TOS in contrast to the alumina-supported catalysts that show changes in most of the followed parameters, particularly during the first 24 h on stream (Figure 4).

In line with the conclusions based on the elemental composition of products, the lab-made $NiMo/Al_2O_3$ (Exp_4/L) together with the commercial catalyst of Exp_2/C showed the most significant improvement of the

Downloaded from pubs.acs.org/ascecg/article-pdf/8/40/15149/6712707/acssuschemeng.0c03896.pdf by UNIV CHEMISTRY & TECHNOLOGY PRAGUE user on 26 October 2026

https://dx.doi.org/10.1021/acssuschemeng.0c03896
ACS Sustainable Chem. Eng. 2020, 8, 15149−15167

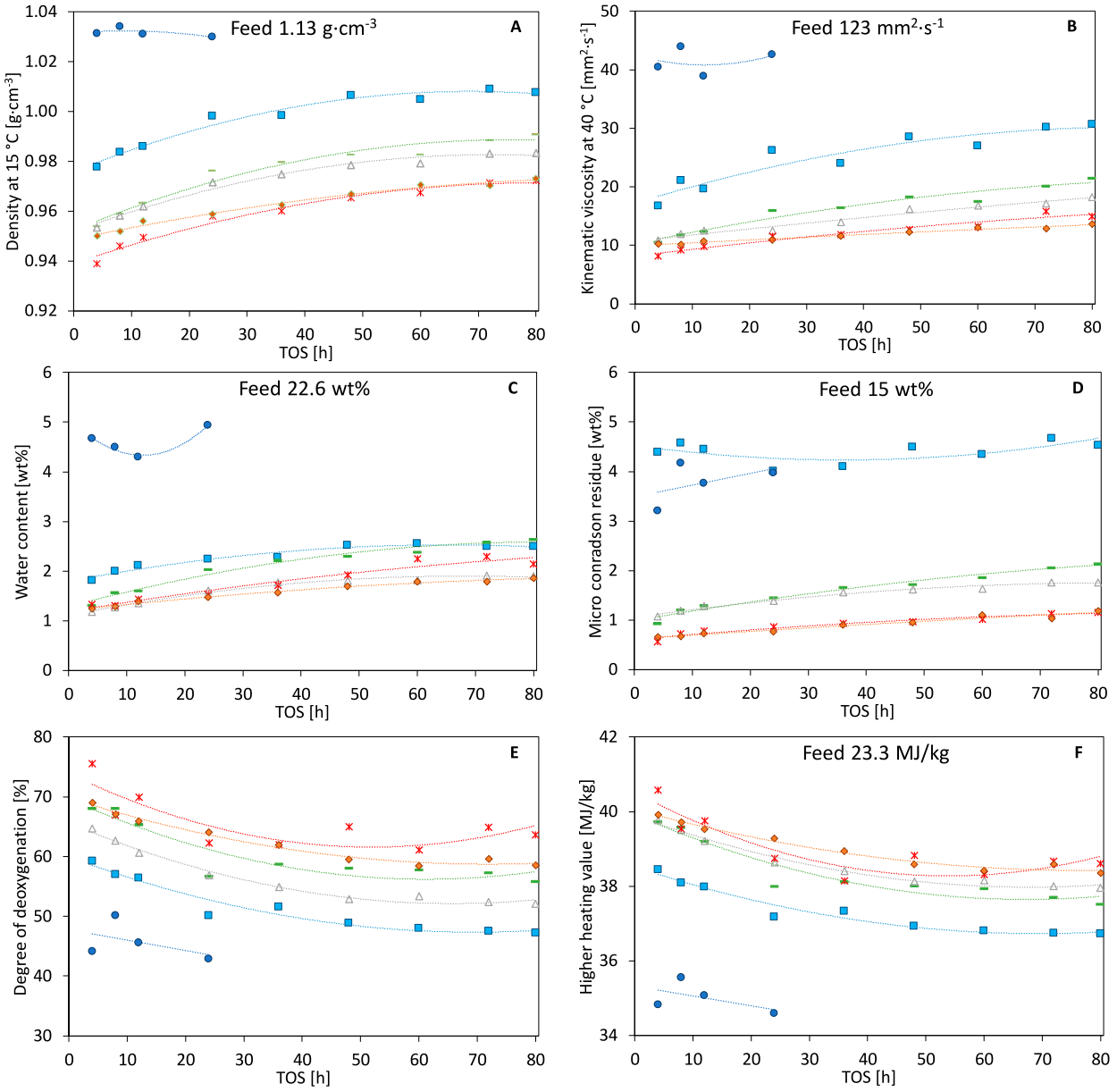


Figure 4. Physicochemical properties of the liquid products (organic phase). A − density at 15 °C [g·cm^{-3}], B − kinematic viscosity at 40 °C [mm^2·s $^{-1}$], C − water content [wt %], D − micro Conradson residue [wt %], E − degree of deoxygenation [%], and F − higher heating value [MJ/kg]. ■ (blue) Exp_1/C, ◊ (orange) Exp_2/C, Δ (gray) Exp_3/L, ∗ (red) Exp_4/L, ● Exp_5/L, − (green) Exp_6/L.

bio-oil properties and highest stability of catalyst activity in the whole range of the TOS. After 80 h, the density increase was only 0.02 g·cm^{-3}, and viscosity increased only by 4 mm^2·s^{-1}. Importantly, the micro Conradson carbon residue was less than 1 wt % after 80 h, while in the other experiments, it reached 4 wt % after 80 h (Figure 4).

On the other hand, the commercial catalyst (Exp_1/C), showing the highest HDS activity, performed the worst among the alumina-supported catalysts (Figure 4). Not only it showed the lowest initial deoxygenation activity but also the activity deteriorated with the increasing time-on-stream as did the product properties (Figure 4). Most interestingly, the products had a very high micro Conradson carbon residue, comparable to the products obtained by upgrading bio-oil over NiMo/SiO_2 (Figure 4). The higher heating value for most products was in the range ca. 38−41 MJ·kg^{-1}, i.e., it almost doubled compared to bio-oil, and was rather close to the HHV of diesel (ca. 45 MJ·kg^{-1}). Priharto et. al[18] obtained similar but lower values of HHV (38.8 MJ·kg^{-1}) after hydrotreatment of lignin-derived pyrolysis bio-oil over NiMo/Al_2O_3 catalysts after 4 h at 350 °C and 10 MPa pressure in a batch reactor. The dramatic increase in the HHV values is mainly due to partial hydrogenation and deoxygenation that result in changed polarity of the products and, hence, in water separation. A further increase in the HHV could be obtained by a further increase in the severity of reaction conditions to reach a higher degree of deoxygenation.

An important conclusion can be made based on the physicochemical properties of liquid products and composition of lab-made catalysts. Here, it was observed that with the increasing Ni/Mo atomic ratio on alumina-supported lab-made catalysts (Table 2) the liquid product quality decreased (Figure 4) showing higher density, water content, and lower HHV. Thus, the most appropriate Ni/Mo atomic ratio should

Downloaded from pubs.acs.org/ascecg/article-pdf/8/40/15149/6712170/acssuschemeng.0c03896.pdf by UNIV CHEMISTRY & TECHNOLOGY PRAGUE user on 26 October 2026

https://dx.doi.org/10.1021/acssuschemeng.0c03896
ACS Sustainable Chem. Eng. 2020, 8, 15149−15167

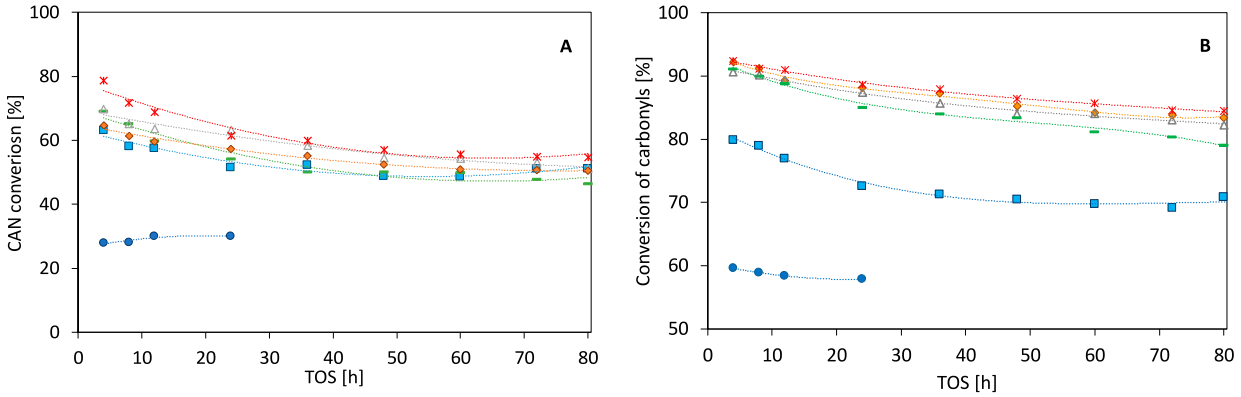


Figure 5. Carboxylic acid number (CAN) conversion [%] of hydrogenated products (A) and conversion of carbonyls [%] (B). ■ (blue) Exp_1/C, ◊ (orange) Exp_2/C, Δ (gray) Exp_3/L, ∗ (red) Exp_4/L, ● Exp_5/L, − (green) Exp_6/L.

be close to 0.30 so the product quality can be comparable or even better than products from the commercial catalyst.

Chemical Composition of Liquid Products. *Carboxylic Acid Number and Amount of Carbonyls.* The application of the total acid number (TAN) method, which is commonly used to determine naphthenic acids in crude oils, to bio-oils is negatively influenced by bio-oil chemical complexity and the presence of different oxygenated compounds. The presence of very weak acids (e.g., phenolic compounds) can affect TAN results, due to the second titration end point, but these compounds do not contribute to corrosion in the petroleum industry.[38,39] Thus, it is more suitable to use a selective method to determine only carboxylic acids—Carboxylic Acid Number (CAN)—for the analysis of bio-oils and products of their upgrading. The results can be also expressed in milligrams of KOH needed for the titration of 1 gram of a sample, as it is reported in the TAN method.

Conversion of compounds that contribute to the CAN value, i.e., carboxylic acids (see eq 2 on page S-4 in the SI), is denoted as CAN conversion and presented in Figure 5A. Nevertheless, it should be mentioned that the concentration of carboxylic acids (mainly acetic acid) during bio-oil hydrotreatment is also affected by their distribution between the aqueous phase and the hydrogenated bio-oil. Details on the distribution of various organic compounds between aqueous and organic phases can be found in ref 6. Hence, the data presented in Figure 5A should be used only for comparing different catalysts and not for evaluation of absolutes values. The content of acetic acid (according to GC-MS) in upgraded products is presented in the SI in Figure S4.

Exp_4/L showed the highest conversion of CAN at the 4-h TOS equals 82% (feed bio-oil 52 mg KOH·g^{-1}) which is approximately five times less than for raw bio-oil. Surprisingly, the CAN conversion of the first sample in Exp_2/C was as high as 68%, although the products obtained over this commercial catalyst had similar physicochemical properties as products of Exp_4/L (Figure 5). In line with the other properties, the other commercial catalyst (Exp_1/C) showed the worst performance, i.e., the lowest CAN conversion, among the alumina-supported catalysts, while NiMo/SiO_2 exhibited the lowest CAN conversion among all tested catalysts 32% (ca. 38 mg KOH·g^{-1}, Figure 5). Moreover, while the CAN conversion values decreased with the TOS for all alumina-supported catalysts (from ca. 82−65 to about 65−55%), the CAN conversion over NiMo/SiO_2 was constant over 24 h on stream at a value of 28% (Figure 5A). Thus, the upgraded bio-oil products could be integrated into a crude-oil refinery (limit of TAN ca. 2 mg KOH·g^{-1}) only after a high dilution with a crude-oil fraction to obtain an appropriate feedstock for further upgrading. Also, the final upgraded product can be distilled (more in the section Distillation of Upgraded Products and Characterization of Distillates) to change the distribution of acids. Specifically, the acids will be concentrated in the lighter distillates, whereas the distillation residue will contain only traces of remaining acids.

Even a more significant decrease than in the case of carboxyl groups was observed for the total content of carbonyls determined by the Faix titration method (Figure 5B). Based on our previous results, we can assume that distribution of carbonyls to the aqueous phase of the product is negligible compared to distribution to the organic phase.[4] All lab-made alumina catalysts showed very close results as the commercial catalyst in Exp_2/C. The carbonyl conversion decreased from the initial 92% to 84% after 80 h on stream (Figure 5B), which can be ascribed to the catalyst deactivation. Similar carbonyl conversion was published by Zacher et al.[23] They hydrotreated an oak bio-oil over the Ru/TiO_2 catalyst under 12 MPa and 140 °C with LHSV 0.23 h^{-1}. However, the Ru catalyst was poisoned by sulfur present in bio-oil, while NiMoS catalysts should be resistant to high sulfur concentration. The other commercial catalyst (used in Exp_1/C) exhibited the worst activity in the carbonyl conversion (only 72% after the 40-h TOS), but on the other hand, during the next 40 h, the content of carbonyls in the products was stable, in contrast to the other experiments using alumina-supported catalysts. In agreement with the other results, NiMo/SiO_2 exhibited the lowest conversion of carbonyls (ca. 58%) though stable one (Figure 5B).

FTIR Spectroscopy with Principal Component Analysis. FTIR spectroscopy was utilized as a screening method for a rapid comparison of the chemical composition of the products of bio-oil hydrotreatment and, thus, an indicator of catalyst deactivation. Compared to other analytical methods, for example NMR, which also provides only screening information and not precise quantification for such a complex matrix as bio-oil, FTIR-ATR is a cheap and robust analytical technique that can give meaningful results in a few seconds/mins. The main advantage of FTIR-ATR measurement compared to other techniques is low operational costs associated with sample preparation. The measured FTIR-ATR spectra of the bio-oil and selected products of the bio-oil hydrotreatment (Exp_4/L) at the start (4 h) and at the end (80 h) of the

Downloaded from pubs.acs.org/ascecg/article-pdf/8/40/15149/6712707/acssuschemeng.0c03896.pdf by UNIV CHEMISTRY & TECHNOLOGY PRAGUE user on 26 October 2026

https://dx.doi.org/10.1021/acssuschemeng.0c03896
ACS Sustainable Chem. Eng. 2020, 8, 15149−15167

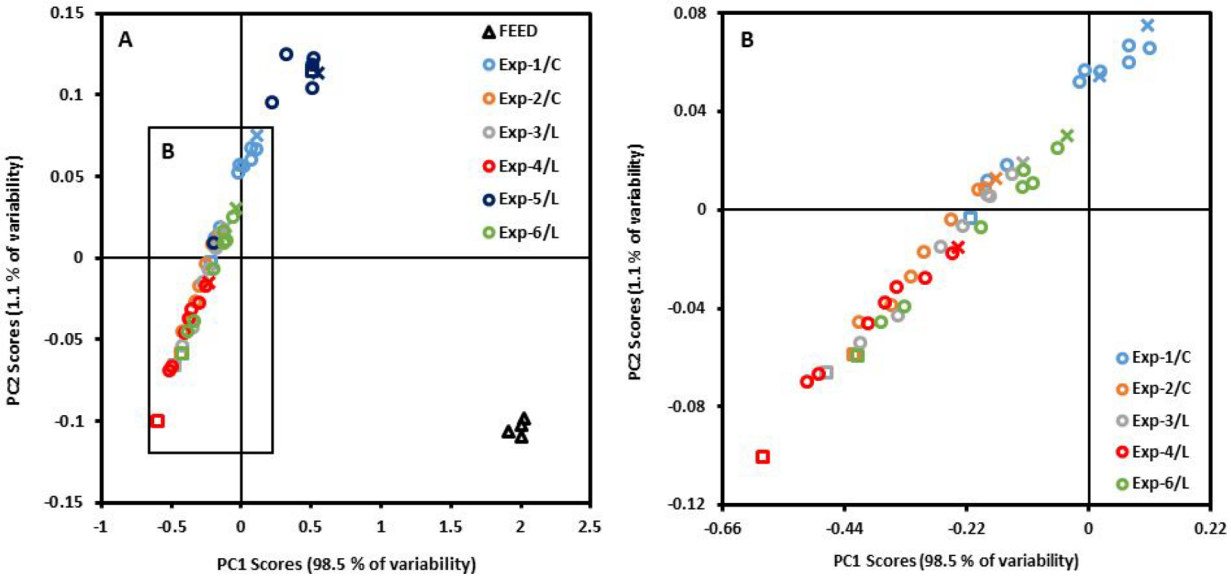


Figure 6. PCA of hydrogenated bio-oil: (A) all hydrogenated products and bio-oil and (B) selected area of products. □ – 4-h TOS, ○ – 8–72-h TOS, × – 80-h TOS.

experiment are presented in SI Figure S5. A detailed interpretation of the straw bio-oil infrared spectrum and spectra of the products obtained by the bio-oil hydrotreatment together with a detailed description of PCA was presented previously.[7] As can be seen in Figure 6, the absorbance of all bands present in the spectrum of the bio-oil is higher than the absorbance of the same bands in the spectra of the hydrotreated products except the bands belonging to the methyl and methylene groups stretching vibrations (region 2992–2795 cm^{-1}). The increase in the absorption intensity of these bands can be attributed to the increasing content of such groups as a result of the, for example, hydrodeoxygenation of C═O (1697 cm^{-1}) (aldehydes, ketones, carboxylic acids), water separation, and double bonds hydrogenation. If we compare the spectra of the first and the last product from the bio-oil hydrotreatment, an obvious quality decrease (higher O–H and C═O absorbance bands) can be observed. These chemical changes are closely associated with the catalyst deactivation due to its long-term exposure to water, acids, and reactive compounds that could form coke residues on the catalyst surface and prevent access to active sites. The measured infrared spectra are complex, and it would be difficult to use them directly for rapid monitoring of the changes in product composition and hence the catalyst performance during the real time of the experiment. Therefore, the IR spectra were utilized as input data for the principal component analysis (PCA) that allowed extracting the most important information for a simple catalyst comparison based on the variations in the quality of the bio-oil hydrotreatment products. The results of the PCA analysis are shown in Figure 6.

The first two principal components (PC1 and PC2) captured 99.6% of the original data (spectra) variability, so only data regarding these principal components will be discussed further. The plot of PC1 vs PC2 scores of all samples is shown in Figure 6A, while Figure 6B presents a closer look at the most important part of the PC1 vs PC2 scores plot. As it can be seen in Figure 6A, two distinguishable clusters of points were formed. One cluster is composed solely from points of feeds (bio-oil), the other one contains points belonging to the products of the bio-oil hydrotreatment. The separation of the points belonging to the feeds from the other samples can be mainly attributed to PC1. Although utilization of PC2 also supported the separation of the feeds points, the separation is not so clear because PC2 scores values of feeds are similar to PC2 scores of several products, especially the Exp_4/L 4-h TOS which is located in the bottom left corner of the plot. Considering the IR spectrum and physicochemical properties of this sample, the sample showed the highest level of deoxygenation. On the other hand, the products Exp_5/L ($NiMo/SiO_2$), located in the top part of the plot, can be considered as the product with the lowest level of deoxygenation. In other words, PCA screening can be used to evaluate product quality almost online during the experiment. The increase in the severity of reaction conditions during the experiment Exp_5/L (from 4 to 8 MPa and from 340 to 360 °C) was reflected by the shift of the position of the Exp_5/L products points closer to the rest of the better products zoomed in Figure 6B. Nevertheless, even these products obtained at more severe conditions did not match the quality of the products obtained at the beginning of the other experiments.

While the activity of the catalyst used in the experiment Exp_4/L can be considered as the highest, the catalyst used in the experiment Exp_1/C showed the worst activity from all $NiMo/Al_2O_3$ catalysts (as obvious from the position of the PCA scores of products obtained when using these catalysts). Even the product obtained at the beginning of the experiment Exp_1/C had poor quality which was comparable with the quality of the products obtained at the end of the other experiments. Nevertheless, a flushing of the catalyst bed with a polar solvent after 80 h on stream and restarting of the hydrotreatment process led to the a partial recovery of the catalyst activity (marked by a blue cross in the middle of O-marks of the product from Exp_1/C in Figure 6). So, this simple technique can be used to prolong catalyst activity. A detailed discussion about PCA dependency on the wavenumber from the IR spectra belonging to the exact functional

Downloaded from pubs.acs.org/ascecg/article-pdf/8/40/15149/6712707/acssuschemeng.0c03896.pdf by UNIV CHEMISTRY & TECHNOLOGY PRAGUE user on 26 October 2026

https://dx.doi.org/10.1021/acssuschemeng.0c03896
ACS Sustainable Chem. Eng. 2020, 8, 15149–15167

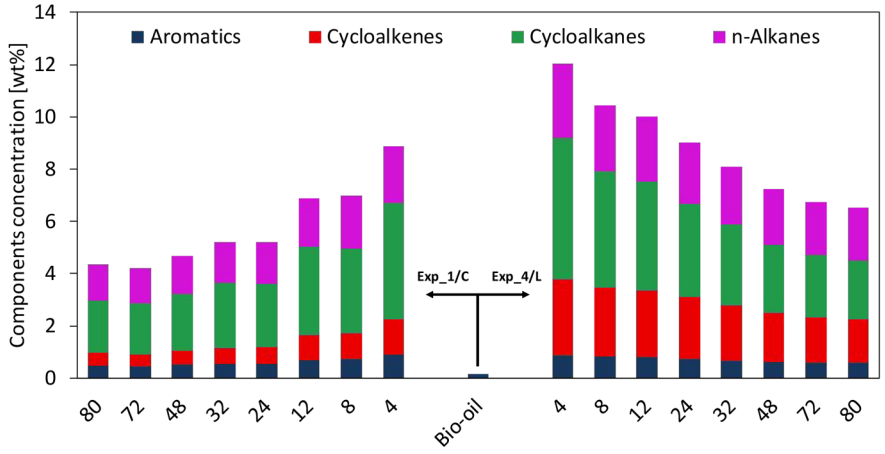


Figure 7. Content of aromatics (dark blue), cycloalkenes (red), cycloalkanes (green), and *n*-alkanes (purple) in hydrotreated bio-oil (organic phase) from Exp_1/C and Exp_4/L experiments.

group/bond is presented in the text of the Supporting Information (pages S-7 and S-8) and in Figure S6.

Catalyst stability comparison can be based on the distance of the point belonging to the product obtained at the beginning of an experiment and at the end of the experiment. Since the shortest distance between the first and the last product PCA scores was observed in the case of the experiment over the commercial $NiMo/Al_2O_3$ (Exp_2/C), the catalyst used in this experiment can be considered as the most stable one.

GC-MS Analysis of Organic Products. In this work we did not attempt to quantify all present compounds in bio-oil or in bio-oil products, as we did in our previous study.[4] Instead, we focused on the influence of catalyst deactivation on the concentration of chosen compounds that are highly abundant in bio-oil (syringol, guaiacol, phenol, 4-propylphenol, etc.) and the products of oxygenates transformation, e.g., by demethoxylation, demethylation, or deoxygenation leading to different hydrocarbons. The content of the selected oxygenates and the products of their hydrogenation in reaction products is illustrated in Figure S7. However, it should be mentioned that phenolic compounds are more resistant to deoxygenation under the used reaction conditions, and their amount increased during hydrotreatment of bio-oil as a consequence of cracking of high-molecular species, such as pyrolytic lignin. For example, the content of phenol was doubled at 340 °C over NiMo catalysts compared to bio-oil, and the content of 3,4-propylphenol was even ten times higher in upgraded bio-oil according to our previous research.[4] The increased content of some phenolics, such as 4-propylguaiacol and 4-ethylguaiacol (Figure S7) with the increasing TOS, reflects the catalytic activity loss and inability to fully hydrogenate these molecules (primary pyrolysis products). Also, decreasing phenol and cresol content (Figure S7F,H), which are secondary products, indicates catalytic activity loss due to suppressed cracking and demethoxylation reactions. The relatively high content of phenolic compounds in upgraded bio-oil (Figure S7) can be a consequence of both their refractory nature during deoxygenation as well as their additional formation from lignin oligomers present plausibly in bio-oils.

Reaction selectivity and degree of deoxygenation in catalytic conversion of phenolics strongly depend on the catalyst type and its properties.[40] Noble metal catalysts are suitable for efficient hydrogenation of aromatic rings and demethoxylation/hydrodeoxygenation of phenols. In particular, Pd, Ru, Pt, and Rh supported on C, Al_2O_3, and ZrO_2 have been mostly used to hydrodeoxygenate phenolic model compounds to produce aromatic hydrocarbons and saturated cyclic compounds through hydrogenolysis and hydrogenation mechanisms. Also, some reduced transition metals such as Ni, Cu, Co, and Mo, which can replace expensive noble metals, also showed good performance in phenol hydrodeoxygenation to hydrocarbons.[41−47]

From the fuel production point of view, hydrocarbons are the most desirable components; therefore, we present the content of hydrocarbons in the hydrotreated bio-oil. The content of analyzable hydrocarbons (aromatics, cycloalkenes, cycloalkanes, and *n*-alkanes) in the worst (Exp_1/C) and the best (Exp_4/L) products prepared over alumina-supported catalysts is shown in Figure 7. The data for other catalysts are summarized in Figure S8. The initial content of hydrocarbons in the raw bio-oil was ca. 0.14 wt %, predominantly in the form of aromatic compounds. However, already in the first hydrotreated product (Exp_2/C 4 h), the concentration of hydrocarbons significantly increased to 12 wt % in the form of alkanes, cycloalkenes, cycloalkanes, and aromatics. The concentration of *n*-alkanes increased from 0 wt % in raw bio-oil up to 2.9 wt % in the 4-h products and decreased to ca. 2.2−2.5 wt % after 80 h over the best catalysts (see Figure 7). Alkanes were created predominantly by deoxygenation of organic acids and ketones that were highly represented in the raw bio-oil.[4] Isoalkanes were found in hydrotreated bio-oil as well.

The high increase in cycloalkenes and cycloalkanes in the upgraded bio-oil was very important as it leads to a decrease in the product polarity and, consequently, to a better miscibility with crude-oil distillates and higher fuel value. It can be expected that cycloalkenes are formed by the dehydration of cyclohexanols (Figure S7), i.e., products of phenol hydrogenation, whereas cycloalkanes are the products of cycloalkene hydrogenation. Although the concentration of cyclohexanol was relatively low (<0.1 wt %), its presence was very important for understanding the reaction pathways of phenol hydrogenation (Figure S9). Also, cyclohexanol concentration increased with the time-on-stream as a consequence of catalyst activity loss.

While raw bio-oil contained no cycloalkenes and cycloalkanes, in the first products (Exp_4/L 4-h TOS) their concentration was up to 3 and 5 wt %, respectively, over

https://dx.doi.org/10.1021/acssuschemeng.0c03896
ACS Sustainable Chem. Eng. 2020, 8, 15149−15167

Downloaded from pubs.acs.org/ascecg/article-pdf/8/40/15149/6712707/acssuschemeng.0c03896.pdf by UNIV CHEMISTRY & TECHNOLOGY PRAGUE user on 26 October 2026

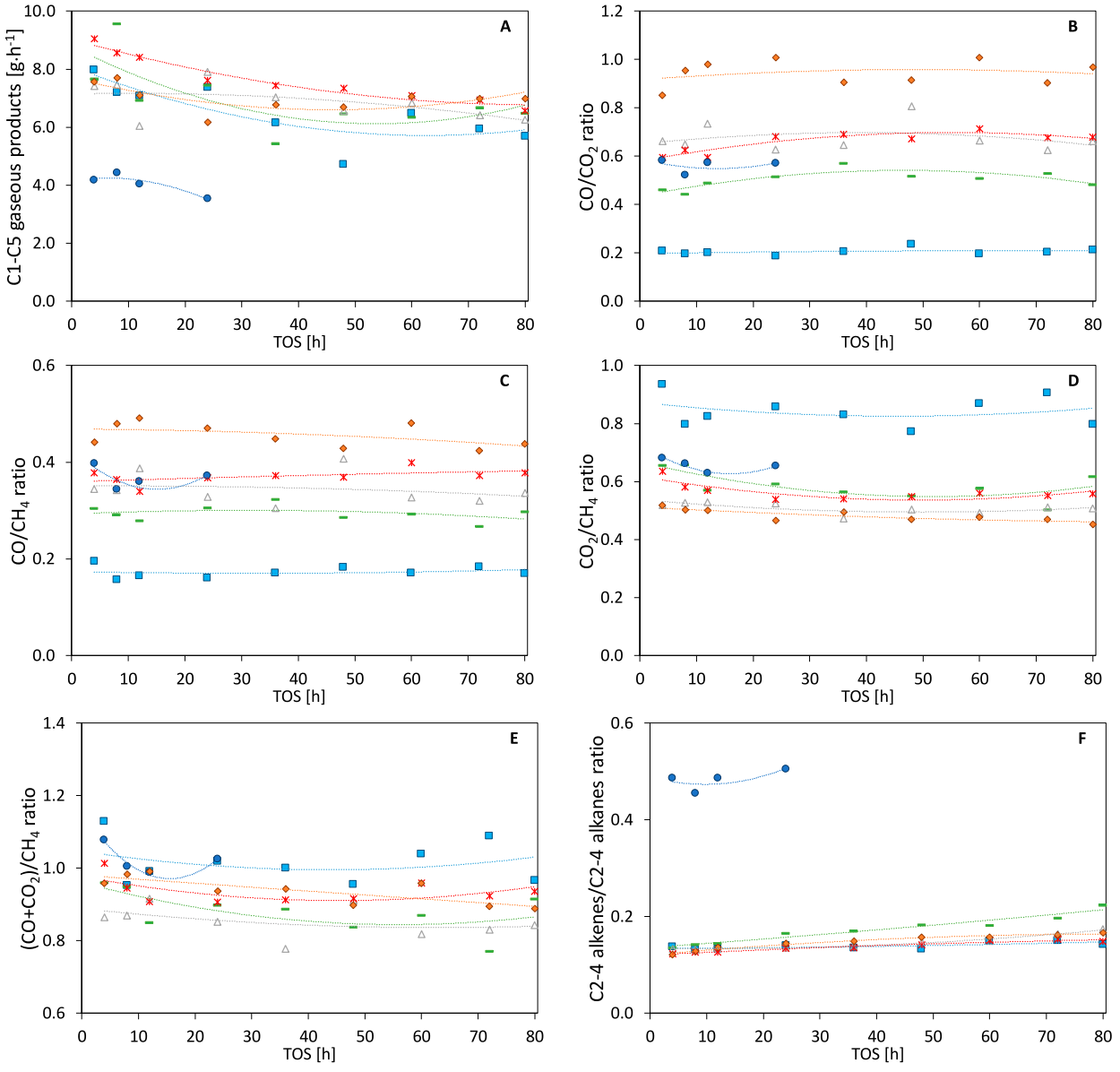


Figure 8. Main compounds in reactor off-gas. (A) − C1−C5 gaseous products flow g·h^{-1}, (B) − CO/CO_2 ratio, (C) − CO/CH_4 ratio, (D) − CO_2/CH_4 ratio, (E) − $(CO+CO_2)/CH_4$ ratio, (F) − C2−4 alkanes/C2−4 alkenes ratio. ■ (blue) Exp_1/C, ◊ (orange) Exp_2/C, Δ (gray) Exp_3/L, ∗ (red) Exp_4/L, ● Exp_5/L, − (green) Exp_6/L.

Table 4. List of Main Hydrocarbons in the Product from Exp_1/C and Exp_4/L with the 4-h TOS

aromatics	wt %	cycloalkenes	wt %	cycloalkanes	wt %	*n*-alkanes	wt %
			Exp_1/C				
toluene	0.12	methylcyclopentene	0.28	ethylcyclohexane	0.77	heptadecane	0.36
ethylbenzene	0.12	cyclohexene	0.17	methylcyclopentane	0.63	pentadecane	0.28
m-/*p*-xylene	0.08	methylcyclohexene	0.16	cyclohexane	0.56	hexane	0.18
methylindane	0.08	propylcyclohexene	0.12	methylcyclohexane	0.52	octacosane	0.16
tetralin	0.06	ethylcyclohexene	0.12	propylcyclohexane	0.51	heptane	0.12
			Exp_4/L				
toluene	0.11	methylcyclopentene	0.58	methylcyclopentane	1.09	heptadecane	0.53
ethylbenzene	0.11	cyclohexene	0.40	ethylcyclohexane	0.81	pentadecane	0.42
m-/*p*-xylene	0.07	methylcyclohexene	0.38	cyclohexane	0.67	hexane	0.25
methylindane	0.07	propylcyclohexene	0.31	propylcyclohexane	0.56	octacosane	0.13
tetralin	0.06	ethylcyclohexene	0.28	methylcyclohexane	0.54	tridecane	0.11

alumina-supported catalysts (see Figure 7). It gradually decreased to 2 and 2.6 wt % for cycloalkenes and cycloalkanes, respectively, after 80 h (see Figure 7) due to catalyst deactivation. Interestingly, the ratio of cycloalkenes to

Downloaded from pubs.acs.org/ascecg/article-pdf/8/40/15149/6712170/acssuschemeng.0c03896.pdf by UNIV CHEMISTRY & TECHNOLOGY PRAGUE user on 26 October 2026

https://dx.doi.org/10.1021/acssuschemeng.0c03896
ACS Sustainable Chem. Eng. 2020, 8, 15149−15167

cycloalkanes over the commercial catalyst $NiMo/Al_2O_3$ used in Exp_1/C was significantly lower than over the other alumina-supported catalysts (<0.3 vs >0.7, Figure 8). This suggests a better hydrogenation activity of this catalyst. The data for $NiMo/SiO_2$ reveal its very poor hydrogenation activity as virtually no cycloalkanes were formed, while the content of cycloalkenes was about 0.4 wt %, only slightly less than in Exp_1/C.

Finally, after bio-oil hydrotreatment, the content of aromatics increased to ca. 0.9 wt % in the best products (Exp_4/L 4-h TOS) and then slightly decreased to ca. 0.65 wt % after 80 h due to catalyst deactivation and thus having a reduced deoxygenation activity (Figure 7). All other catalysts (except for $NiMo/SiO_2$) showed a similar performance with respect to the formation of aromatic compounds. The concentration of aromatics increased only marginally over $NiMo/SiO_2$ (to less than 0.2 wt %), but their concentration did virtually not decrease with the TOS, which is in line with the findings concerning product properties.

The main compounds from hydrocarbon groups, which were discussed above (aromatic, cycloalkenes, cycloalkanes, and *n*-alkanes), are presented in Table 4. The composition of aromatics for both catalysts was similar. The main difference was in the content of saturated hydrocarbons, where the lab-made alumina-supported catalyst (Exp_4/L) showed a higher content of cycloalkanes and *n*-alkanes.

Gaseous Products. Since bio-oils consist of hundreds of oxygenated compounds (phenols, alcohols, carboxylic acids, etc.), deoxygenation reactions take place during the hydrotreatment. Among the deoxygenation reactions, decarbonylation and decarboxylation reactions resulting in the formation of C1 gases are the key reactions contributing to gaseous product formations. Moreover, hydrodeoxygenation of short-chain aldehydes, ketones, acids, and esters results in the formation of C2−C4 gaseous products as well. Consequently, carbon monoxide, carbon dioxide, and hydrocarbons C1−C4 were the main components of gaseous reaction products. Although the main component of outlet gases was hydrogen (ca. 95 vol %), its content is not presented as it was used in excess in the reactions. Moreover, cracking and dealkylation reactions may afford light gaseous hydrocarbons as well.

The production of gaseous products, thus, reflects the catalyst activity and its changes with the increasing TOS. In line with the previous conclusions, the silica-supported catalyst is much less active as the productivity of C1−C5 products is only 50% of that observed for the alumina-supported catalysts. Moreover, it can be observed (Figure 8A) that the productivity of gaseous products declines with the increasing TOS, i.e., as the catalyst activity deteriorates. Considering the precision of the determination of the productivity of gaseous products, the differences among the alumina-supported catalysts are not too significant; nonetheless, catalysts used in Exp2/C and Exp4/L can be described as the most active ones among the alumina-supported catalysts, which is also in agreement with the other results.

Taking into account the bio-oil composition, decarbonylation of aldehydes (and to a much lesser extent of ketones) and decarboxylation and decarbonylation of acids can be expected as primary reactions yielding COx during bio-oil hydrotreatment. They can be accompanied by demethylation and demethoxylation, i.e., primary reactions of methoxyphenol conversion yielding CH_4 and CH_3OH, respectively. The consecutive reactions of these primary products include hydrogenation (including methanation) of COx affording CO and CH_4, hydrogenation of methanol to methane, and water−gas shift and reversed water−gas shift reactions of CO and CO_2, respectively, take place under the bio-oil hydrotreatment conditions. The water−gas shift reaction of CO in the presence of a sulfided NiMo catalyst was previously studied; it was reported that at temperatures above 300 °C CO shows high conversion to CO_2 (ca. 85%).[48,49] Consequently, an unequivocal interpretation of the gaseous product composition, particularly of the C1 product distribution, is extremely challenging if not even impossible. Thus, we have limited the following discussion to describing the observed dependencies rather than drawing not fully substantiated conclusions.

The highest CO/CO_2 ratio in gaseous products has been observed for the experiment Exp_2/C, and the lowest ratio has been observed for Exp_1/C. Both catalysts were commercial but showed a different performance. Also, a slight increase in the CO/CO_2 ratio with the time-on-stream indicates the loss of catalytic activity. This could suggest either that CO is the primary product and its conversion to CO_2 (via WGS) is suppressed or that the decarboxylation reactions are suppressed more than decarbonylation reactions. Considering the changes in liquid product composition, in particular CAN and carbonyl conversion as a function of the TOS (Figure 5), it can be seen that the drop in CAN conversion is more significant that the decrease in carbonyl conversion. Thus, the increase in the CO/CO_2 ratio reflects the lower decarboxylation catalyst activity. In the case of the catalyst Exp_1/C, a very low CO/CO_2 ratio can be observed (Figure 8B) indicating a possible high extent of the WGS reaction (as a much higher decarboxylation activity is not supported by the liquid phase data (Figure 5A) or lower decarbonylation activity, which can be indeed observed in Figure 5B). At the same time, this catalyst showed also the lowest methanation activity CO_x, which is supported by data of CO_2/CH_4 and $(CO+CO_2)/CH_4$ ratios (Figure 8D,E). If we correlate physicochemical properties of liquid products with the ratio CO/CO_2, we can suggest that, in the case of $NiMo/Al_2O_3$ catalysts, the higher CO and the lower CH_4 production are observed the better liquid product quality is obtained.

C2−C4 hydrocarbons were a very important part of the gaseous products. Kadawarti et al.[22] reported increasing yields of C2−C4 acids over the NiMo catalyst with the reaction temperature as a product of the cracking of the side chains of sugar-derived oligomers. Part of these carboxylic acids can be converted into C2−C4 hydrocarbons at temperatures higher than 300 °C. In our hydrotreatment experiments, C2−C4 alkanes were the most abundant hydrocarbons (except for CH_4) in off-gases. It is visible from Figure 8F that the (C2−C4 alkenes)/(C2−C4 alkanes) ratio for alumina-supported catalysts is lower than 0.2 at the time-on-stream of 4 h. It points to high hydrogenation activity of alumina-supported catalysts for double bond saturation in, for example, hydrodeoxygenation of propionic acid, propyl alcohol, and acetone to propane/propene or butanoic acid to butane/butene. However, the (C2−C4 alkenes)/(C2−C4 alkanes) ratio increased with the time-on-stream (Figure 8F) as a consequence of the decrease in catalytic activity to hydrogenation/saturation of the C2−C4 olefins. Also, this ratio for the silica-supported catalyst was 3 times higher than for the alumina-supported catalyst, showing much lower hydrogenation activity of the silica-supported catalyst, Exp_5/L (Figure 8F). Among the alumina-supported catalysts, there are

Downloaded from pubs.acs.org/ascecg/article-pdf/8/40/15149/6712707/acssuschemeng.0c03896.pdf by UNIV CHEMISTRY & TECHNOLOGY PRAGUE user on 26 October 2026

https://dx.doi.org/10.1021/acssuschemeng.0c03896
ACS Sustainable Chem. Eng. 2020, 8, 15149−15167

virtually no differences in the hydrogenation of C2−C4 olefins with the TOS apart from the catalyst used in Exp6/L that showed a lower hydrogenation activity at the end of the experiment than the others (Figure 8F).

There are two points of view in the presence of C2−C4 hydrocarbons in gaseous products: their higher concentration indicates a higher catalytic activity; on the contrary, it also shows that energy-rich hydrocarbons are lost from the desired liquid product. Thus, based on the second statement, it would be more useful to have C2−C5 compounds in the product in the form of alcohols, which can be used as a component in a gasoline pool and as octane boosters (ethanol and propyl alcohol). An alternative use of the C2−C4 hydrocarbons is their recovery from the off-gases and their use in a refinery as a feedstock or as fuel gas.

Spent Catalyst. Coke Deposit. The propensity of bio-oils to coking due to the presence of very reactive compounds is widely recognized as the major reason for catalyst deactivation.[50] Therefore, all spent catalysts were analyzed to determine the carbon content in them along the catalyst bed to determine carbon content profiles. The results are presented in Figure 9. The highest carbon content was found in a place of contact of raw bio-oil and hot catalyst surface in the first 35 mm depth of the catalyst bed for all catalysts, which reflects the highest coking rate at the top of the catalyst bed due to the highest concentration of the compounds most prone to coking, such as aldehydes or ketones (Figure 9). The catalyst from the experiment Exp_1/C had the highest coke content along the catalyst bed, which can be explained by the longer time-on-stream, 100 h, in comparison with the other experiments using the alumina-supported catalysts (80-h TOS). On the other hand, the experiment with the $NiMo/SiO_2$ (Exp_5/L) was carried out only for ca. 40 h due to its unsatisfactory performance. Consequently, the carbon content on the catalyst was the lowest in this experiment. Interestingly, the alumina-supported catalyst used in Exp_6/L (drying instead of calcination was used after the first impregnation step) had a higher coke content than the other two lab-made catalysts prepared by two-step impregnation with calcination after the first step (Exp_3/L) and coimpregnation (Exp_4/L). Also, the physicochemical properties of the liquid products from the experiment Exp_6/L were the poorest among the lab-made alumina-supported catalysts and were close to the commercial catalyst Exp_1/C.

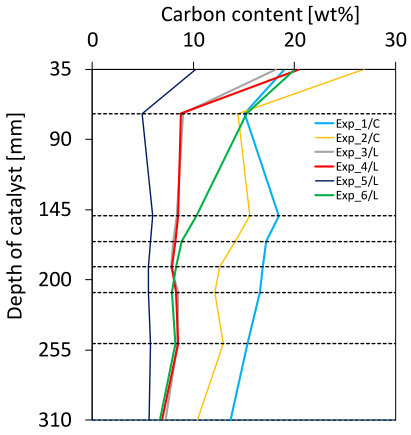


Figure 9. Carbon content on the catalyst depending on the position in the catalyst bed (beginning (top) of the catalyst bed at 20 mm, end (bottom) of the catalyst bed at 320 mm).

Sulfur content on the spent catalyst was also measured by elemental analysis (EA) of the coke+catalyst mixture, and these values can be used for the assessment of sulfur loss during bio-oil hydrogenation. The results of EA of the sulfur content after the experiment are presented in the SI in Figure S10. We measured sulfur content for *in situ* sulfided fresh catalyst Exp_4/L as for the best lab-made catalyst, and the S content was 7.4 wt %. After the hydrogenation experiments, the sulfur content was in the range 7−8 wt % for lab-made catalysts in all reaction zones (Figure S9).

Due to the high water content in bio-oils (typically >20%), its plausible adverse effects on the catalyst performance need to be considered. Laurent et al.[12] widely studied the influence of water on the $NiMoS/Al_2O_3$ catalyst and concluded under hydrotreating conditions it was responsible for the loss of the initial activity of a sulfided NiMo catalyst but did not affect the hydrogenation-hydrogenolysis selectivity. Moreover, water vapor caused a partial crystallization of the γ-Al_2O_3 support into a hydrated boehmite phase.[12] Although a small decrease in the specific surface area was observed, the composition, metal dispersion, and sulfur content of the Mo and Ni phases were virtually unaffected. They concluded that the loss of catalytic activity could be caused by the formation of inactive oxidized nickel species (nickel sulfate) and that these species formed an

Table 5. Properties of Product Distillates

parameter	aqueous phase (AP)	light gasoline (LG)	heavy gasoline (HG)	diesel (D)	distillation residue (DR)
boiling point [°C]	<100	<100	100−200	200−360	>360 °C
yield [wt %][a]	2.0	10.9	9.8	46.5	30.8
water content [wt %]	78.9	0.41	3.73	0.18	LOD[d]
acid distribution [%]	3.5	3.8	54.3	38.4	LOQ[c]
carbonyl distribution [%]	4.6	42.7	33.0	19.6	LOQ[c]
		Elemental Composition, Dry Basis			
carbon [wt %]	10.68	82.66	73.17	80.3	85.18
hydrogen [wt %]	11.39	12.89	10.97	9.95	9.89
nitrogen [wt %]	LOQ[c]	LOQ[c]	LOQ[c]	0.73	1.55
sulfur [wt %]	0.01	0.03	0.03	0.01	0.01
oxygen [wt %]	79.95	6.5	17.8	11.8	5.36
H/C ratio	*b*	1.86	1.80	1.48	1.39

[a]Yields were related to 100%; mass losses were 2.7 wt %. [b]Not calculated due to high water content. [c]LOQ − limit of quantification, CAN 0.1 mg KOH/g, carbonyls 0.01 mmol C═O/g. [d]LOD − limit of detection.

https://dx.doi.org/10.1021/acssuschemeng.0c03896
ACS Sustainable Chem. Eng. 2020, 8, 15149−15167

Downloaded from pubs.acs.org/ascecg/article-pdf/8/40/15149/6712707/acssuschemeng.0c03896.pdf by UNIV CHEMISTRY & TECHNOLOGY PRAGUE user on 26 October 2026

inactive layer on the surface of nickel and molybdenum sulfided particles. As a consequence, access to the active sites would be hindered and/or their quantity reduced, resulting in the observed lower activity that was also claimed by other researchers based on their spectroscopy analysis.[51,52] Importantly, sulfur content in products did not change during hydrogenation and was lower than in the feed.

Distillation of Upgraded Products and Characterization of Distillates. One of the goals of our work was to stabilize bio-oil and prepare a petroleum-refinery compatible feedstock that can be refined in the second step together with crude-oil distillates. However, it is also an opportunity to process hydrotreated bio-oil together with crude-oil in refinery (its distillation and followed upgrading processes).

Nonetheless, for better characterization of final products, we have decided to distill the product from Exp_6/L collected during the 24−32-h TOS into four fractions (with the following boiling point ranges: <100 °C, 100−200 °C, 200−360 °C, and >360 °C) using an automatic distillation apparatus Fischer Technology SPALTROHR©-COLUMNS HMS 500. All distillates were liquid at 25 °C, whereas the distillation residue was solid. A picture of the obtained distillates is presented in SI Figure S11. In the first fraction (bp < 100 °C), the separation of the distillate into an organic (top) and an aqueous phase (bottom) has occurred, while all other fractions from the distillation consisted of a single organic phase. The yields of all fractions, their elemental composition, and water content are given in Table 5 together with information on the distribution of acids and carbonyls among the different distillation cuts. The middle distillate (diesel fraction, 200−360 °C) was the main product and made up 47 wt % of the hydrotreated product.

The estimated yield of gasoline (<200 °C), diesel (200−360 °C), and distillation residue (>360 °C) by the SIMDIS method was 23, 43, and 34 wt %, respectively, based on the distillation range of hydrogenated bio-oil analysis. The respective yields obtained by the distillation were 23, 47, and 31 wt % (Table 5). Thus, it can be concluded that the SIMDIS method can be used to predict the product yields very well.

The distillation range of the hydrotreated bio-oil fractions determined from SIMDIST data is shown in Figure 10. The distillation ranges of all fractions overlapped, as a result of the small scale of the distillation apparatus used. The distillation temperature ranges determined by SIMDIST were much broader than the target range in all the fractions. The end points (EP) of three distillates determined by SIMDIST were well above the target end point temperature. Christensen reported overlapping of distillation ranges of distillates.[39]

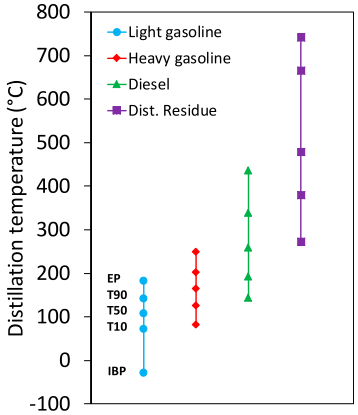


Figure 10. Distillation range of hydrotreated bio-oil fractions (by SIMDIST).

Composition of Distillates. CAN, Carbonyls by Faix, and GC-MS Analysis. The detailed analysis of the individual fractions obtained by distillation has clearly shown that the distribution of the different types of oxygenates is uneven. While the maximum of acids is in the boiling point range 100−360 °C, the carbonyl-containing compounds are mostly accumulated in the lighter fractions (<200 °C, Table 5). More than 50% of all acids were concentrated in the heavy gasoline fraction (100−200 °C). Similar conclusions about the acidity distribution for hydrotreated products with a comparable amount of oxygen were reported by Christensen et al.[38] who showed that acids are present mainly in the lighter distillates. They compared the TAN and CAN methods for the determination of the acidity of the individual distillates. For all distillates except jet fuel (182−260 °C), they obtained the same results for both TAN and CAN, demonstrating the presence of phenols solely in the jet fuel fraction. These conclusions agree with ours where most of the volatile phenols were present in the fractions 100−200 °C and 200−360 °C, phenol and *o*-, *m*-, and *p*-cresols were present in heavy gasoline, and ethyl- and propylphenols were present in the diesel fraction (Figure 11). The list of identified and quantified compounds in distillates is presented in the SI in Table S2. These compounds are further discussed in the following paragraphs.

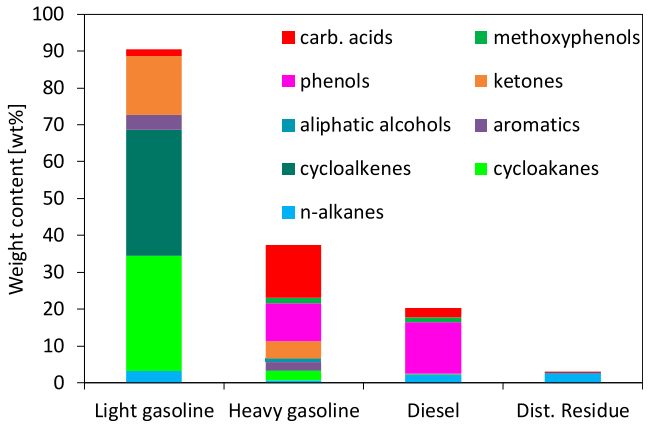


Figure 11. Chemical composition of distillates.

Assuming only carboxylic acids with one functional group (−COOH), it can be approximated that in the boiling range 100−360 °C acids with a carbon number from C1 up to C18 can be present. The list of the main identified acids in hydrotreated bio-oil fractions is listed in Table 6. The measurement of CAN in the distillation residue was limited by the solubility of the sample in isopropyl alcohol, due to the highly aromatic nature of the residue. Therefore, the sample was dissolved in the solvent for Total Acid Number measurements (100:99:1 toluene:isopropyl alcohol:water) to measure the CAN. Nevertheless, the acid content in the distillation residue was lower than the limit of quantification (LOQ).

A slightly different distribution picture was observed for the carbonyl content in distillates. The major part of carbonyls was present in the light and heavy gasoline fractions. The carbonyl

Downloaded from pubs.acs.org/ascecg/article-pdf/8/40/15149/6712707/acssuschemeng.0c03896.pdf by UNIV CHEMISTRY & TECHNOLOGY PRAGUE user on 26 October 2026

https://dx.doi.org/10.1021/acssuschemeng.0c03896
ACS Sustainable Chem. Eng. 2020, 8, 15149−15167

Table 6. List of Identified Carboxylic Acids in Hydrogenated Bio-Oil Fraction wt % (by GC-MS)

compound	aqueous phase	light gasoline	heavy gasoline	diesel	distillation residue
acetic acid	ND[a]	1.09	6.69	0.42	ND[a]
propionic acid	ND[a]	0.34	2.98	0.20	ND[a]
butyric acid	ND[a]	0.25	3.61	0.48	ND[a]
valeric acid	ND[a]	ND[a]	1.04	1.17	ND[a]
palmitic acid	ND[a]	ND[a]	ND[a]	0.21	ND[a]
stearic acid	ND[a]	ND[a]	ND[a]	0.22	ND[a]

[a]ND − nondetected.

compounds detected by the Faix method were predominantly ketones (Table 7). According to Patil et al.,[53] high-molecular-weight pyrolytic lignin compounds, not detectable by GC-MS, contain both aldehyde and ketone groups. However, the carbonyl content in the distillation residue was lower than LOQ (Table 5), showing a high saturation of the high-boiling-point fraction during hydrotreatment.

Although the distillation decreased the complexity of the fractions, the reduction in the complexity was not enough to allow identifying and quantifying all compounds present in the fractions. However, it was possible to determine oxygen distribution in the distillates and to identify these oxygenated compounds by GC-MS. Moreover, hydrocarbons present in the light distillates and their structure could be determined.

Compounds corresponding to nearly 90 wt % of light gasoline were identified by GC-MS (Figure 11). Most of light gasoline was completely deoxygenated and consisted of alkanes, cycloalkanes, and cycloalkenes (70 wt %) (Table 8). The remaining identified compounds were ketones (17 wt %) and carboxylic acids (Tables 6 and 7), which represented 4 wt % of oxygen based on GC-MS data (see Table 6). In Figure 12 and Figure 13 are presented yields and distribution of *n*-alkanes and cycloalkanes in the distillates. They were formed mainly by the hydrotreatment of linear alcohols/ketones and carboxylic acids, which is in agreement with acid distribution in the distillates.

The number of quantified compounds by GC-MS significantly decreased with the increasing boiling point of the fraction and, hence, its increasing complexity. Thus, the wt % of the identified compounds dropped down to about 37 wt % in the case of heavy gasoline, 20 wt % for the diesel fraction, and only ca. 3 wt % in the case of the distillation residue (Figure 11). The heavy gasoline cut (bp 100−200 °C) had the highest content of oxygen (17.8 wt %) in the form of carboxylic acids, carbonyls, and phenolic compounds. Based on the calculation from CAN values, oxygen contribution from carboxylic acids to the total oxygen content should be ca. 7.6 wt %. However, based on GC-MS data, the oxygen content due to carboxylic acids of about 6.5 wt % was determined. Phenols in heavy gasoline contributed ca. 1.7 wt % of oxygen and carbonyls ca. 1 wt % of oxygen (calculated from GC-MS composition). The rest of the oxygen content (8.6 wt %) is hidden in the form of unidentified phenolics and carbonyl-containing compounds. Furthermore, the content of *n*-alkanes in heavy gasoline was the lowest.

In the diesel fraction, oxygen was predominantly present in the form of carboxylic acids (see Table 6), phenols (phenol; *o*-, *m*-, and *p*-cresol; propylphenols), and ketones (see Table 7). As mentioned in Table 6, palmitic and stearic acids were abundant in the diesel fraction. Oxygen contribution by carboxylic acids to the total oxygen in the diesel fraction was ca. 1.2 wt %. Identified phenols contributed to the total oxygen content ca. 1.8 wt %; the main contribution was *m*- and *p*-cresol ca. 0.5 wt % and 3-,4-propylphenol ca. 0.8 wt %. Acetoguaiacone contributed ca. 0.2 wt %. The high content of phenols in the diesel fraction indicates that further upgrading in a refinery together with gas oil distillates may be needed to achieve diesel fuel properties in accordance with the EN 590 standard.

GC-MS was not an ideal method to identify compounds in the distillation residue. Only 3 wt % of the distillation residue could be identified by GC-MS; mainly longer *n*-alkanes (created probably by the coupling of two fatty acids, i.e., ketonization of carboxylic acids, which would be another source of CO_2 in the gas phase, followed by hydrogenation of the resulting ketone) and fatty acids were present. The rest of the distillation residue was created by stigmastane (according to GC-MS) and by high-molecular-weight compounds of pyrolytic lignin. The distillation residue had the lowest oxygen content (5.36 wt %) and the lowest H/C ratio (see Table 5) indicating its high aromaticity. The presence of oxygen in the distillation residue is further discussed in the following section (FTIR Analysis of the Distillates).

FTIR Analysis of the Distillates. The distribution of oxygen over functional groups in the distillates and distillation residue was also estimated by FTIR-ATR analysis (see Figure 14A,B) and compared with the results of GC-MS analysis (Figures 11−13 and Table S2). The spectrum of light gasoline was predominantly composed of absorption bands which can be attributed to vibrations of bonds in hydrocarbons. While stretching vibrations of C−H bonds can be observed in the region 3040−2800 cm^{-1}, bands belonging to deformation vibrations can be found at wavenumbers 1451, 1378, and 728 cm^{-1}. Absorption bands which can be attributed to the vibrations of aromatic structures (1604 and 1508 cm^{-1}) had very low intensity which confirms the results of GC-MS analysis. Also, a small absorption peak 3000 cm^{-1} was observed and can be attributed to olefins (=C−H bonds); however, their presence has not been observed by the GC-MS analysis. The presence of oxygen-containing compounds in light gasoline was confirmed by the band located at 1719 cm^{-1} which can be attributed mainly to the stretching vibration of

Table 7. List of Main Carbonyls Quantified in Hydrogenated Bio-Oil Fraction in wt % (by GC-MS)

compound	aqueous phase	light gasoline	heavy gasoline	diesel	distillation residue
butan-2-one	7.06	5.48	ND[a]	ND[a]	ND[a]
pentan-2-one	4.42	9.13	0.88	0.17	ND[a]
2-methylcyclopentanone	0.11	1.54	3.24	0.19	ND[a]
acetoguaiacone	ND[a]	ND[a]	0.55	0.56	ND[a]

[a]ND − nondetected

Downloaded from pubs.acs.org/ascecg/article-pdf/8/40/15149/6712707/acssuschemeng.0c03896.pdf by UNIV CHEMISTRY & TECHNOLOGY PRAGUE user on 26 October 2026

https://dx.doi.org/10.1021/acssuschemeng.0c03896
ACS Sustainable Chem. Eng. 2020, 8, 15149−15167

Table 8. List of Main Hydrocarbons in the Distillates in wt % (by GC-MS)

aromatics	wt %	cycloalkenes	wt %	cycloalkanes	wt %	*n*-alkanes	wt %
			Light Gasoline				
toluene	1.90	methylcyclopentene	7.15	methylcyclopentane	6.14	heptane	1.50
ethylbenzene	0.90	cyclohexene	5.73	ethylcyclohexane	5.13	hexane	1.07
m-/*p*-xylene	0.64	methylcyclohexene	4.49	cyclohexane	4.20	octane	0.57
			Heavy Gasoline				
methylindan	0.32	ND[a]		propylcyclohexane	1.12	decane	0.17
ethylmethylbenzene	0.26	ND[a]		butylcyclopentane	0.29	undecane	0.15
propylbenzene	0.24	ND[a]		butylcyclohexane	0.22	tridecane	0.13
			Diesel				
methyltetraline	0.07	ND[a]		ND[a]		heptadecane	0.70
methylindane	0.05	ND[a]		ND[a]		pentadecane	0.43
tetralin	0.04	ND[a]		ND[a]		octadecane	0.18
			Distillation Residue				
ND[a]		ND[a]		ND[a]		octacosane	1.10
ND[a]		ND[a]		ND[a]		hexacosane	0.51
ND[a]		ND[a]		ND[a]		heptacosane	0.41

[a]ND − nondetected.

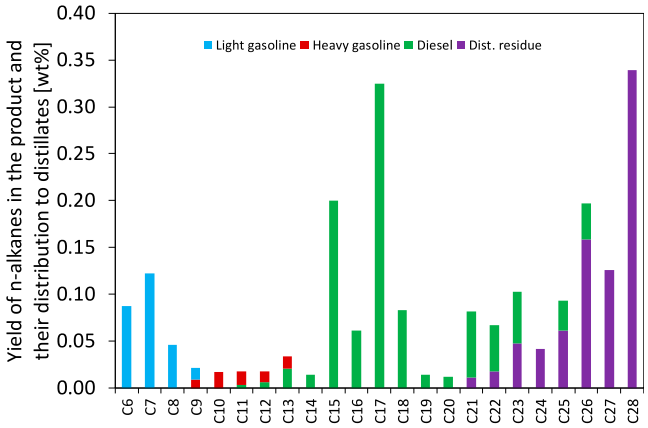


Figure 12. Yields of *n*-alkanes and their distribution in distillates.

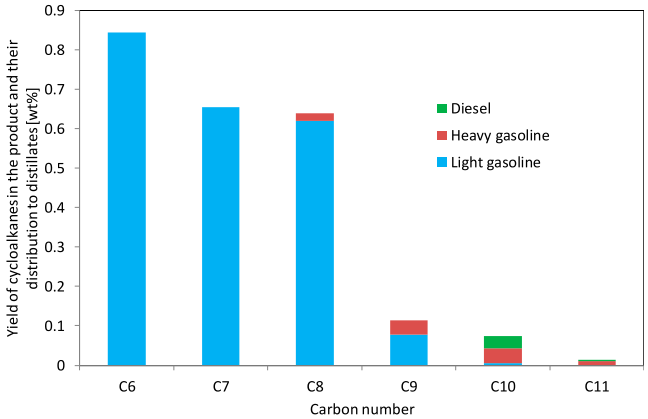


Figure 13. Yields of cycloalkanes and their distribution in distillates.

the carbonyl group of saturated ketones that is in good agreement with results of GC-MS (Tables 6 and 7), for volatile compounds.

The FTIR spectrum of heavy gasoline (Figure 14A) is more complex than that of light gasoline. In addition to the absorption bands assigned to C−H vibrations, the spectrum contains significant signals of other functional groups. The broad absorption band in the range of 3650−2380 cm^{-1} can be predominantly attributed to the stretching vibration of the O−H bond of carboxylic acids (Table 6), phenols (Table S2), and water (Table 5). Carboxylic acids and ketones are clearly seen as a high absorbance peak with a maximum at 1713 cm^{-1}. An increase of aromatic band (1595, 1500, 752, and 694 cm^{-1}) intensity can be observed as well. The overlapped bands in the 1320−1000 cm^{-1} region can be assigned to the oxygen-containing groups present, for example, in phenolic compounds with hydroxyl and methoxy groups, aldehydes, or carboxylic acids.

When increasing the boiling range of the distillate from 100−200 °C to 200−360 °C, increased absorbance in the spectral region at 3630−3200 cm^{-1} was observed (Figure 14B). In comparison with lighter distillates, where the signal in this region was attributed mainly to the O−H stretching vibration of phenols and carboxylic acids, here it was assigned predominantly to O−H stretching vibrations of methoxyphenolic and alkylphenolic compounds. This assumption was based also on the GC-MS data of identified compounds such as *o*-, *m*-, and *p*-cresol, guaiacol, ethylphenol, and 3/4-propylphenol (Table S2), which were highly abundant in the diesel fraction. However, a higher content of such compounds (guaiacol, 4-ethylguaiacol) is also responsible for the increase in the absorption in the spectral region 1320−1000 cm^{-1} where vibrations related to C−O−C bonds can be found. The intensity of the bands in the region 1630−1570 cm^{-1} and at 1515 cm^{-1} belonging to the stretching of the C═C bonds in aromatics (e.g., phenols) was the highest among all distillates which supports the conclusion regarding the high content of phenolic compounds in the diesel fraction. The stretching vibration of the carbonyl group can be also observed in the spectrum of the sample; the absorption bands located at 1717 cm^{-1} can be attributed to saturated ketones and carboxylic acids.

The FTIR spectrum of the distillation residue (bp > 360 °C), presented in Figure 14B, showed the highest absorbance in the spectral region of 3000−2800 cm^{-1} (asymmetrical and symmetrical stretching of the C−H bonds) and very low absorbance caused by the presence of C═O (1717 cm^{-1}). Importantly, that absorption of the methylene group was much higher than that of methyl groups, showing that the distillation residue consists mostly of compounds with a complex cyclic

Downloaded from pubs.acs.org/ascecg/article-pdf/8/40/15149/6712707/acssuschemeng.0c03896.pdf by UNIV CHEMISTRY & TECHNOLOGY PRAGUE user on 26 October 2026

https://dx.doi.org/10.1021/acssuschemeng.0c03896
ACS Sustainable Chem. Eng. 2020, 8, 15149−15167

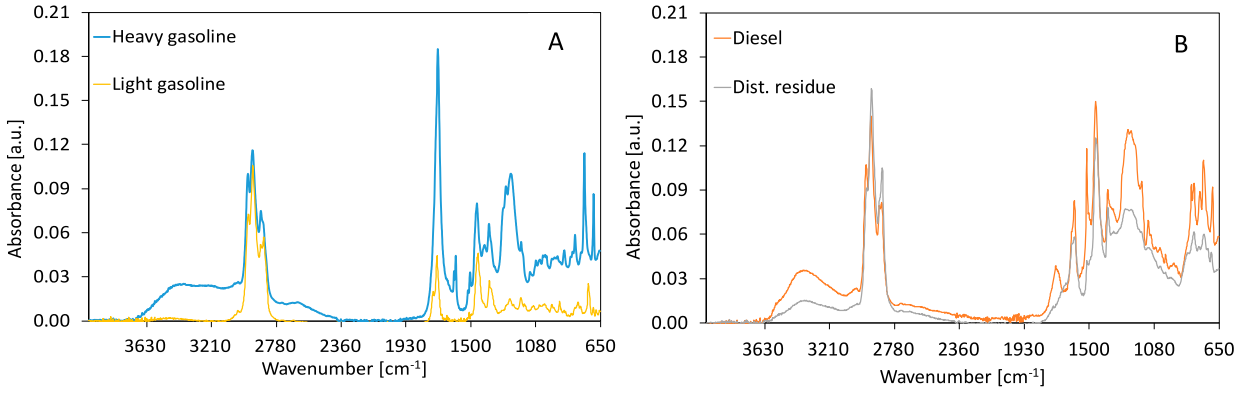


Figure 14. FTIR spectra of light-heavy gasoline (A) and diesel-distillate residue (B) from product distillation.

structure. Compared to the diesel fraction, absorption in the region 1630−1570 cm^{-1} and at 1515 cm^{-1} belonging to the stretching of the C═C bonds in aromatics was much lower, concluding that the distillation residue had more saturated compounds with a carbon number higher than 21 (see Figure 12).

The intensity of phenolic and acidic O−H stretching bands is lower in comparison with the diesel fraction. Relatively high absorption bands can be observed in the region of 1320−1000 cm^{-1} which can be attributed to the content of aromatic esters, ethers, phenolic, and methoxy compounds. It can be assumed that most of the oxygen in the residue is present in heavy molecular structures such as stigmastane (identified by GC-MS) or pyrolytic lignin (or its partially saturated products) in the form of side hydroxyl groups that absorb in the region 3600−3200 cm^{-1}. Negligible intensity of the carbonyl group and a rather low intensity of other oxygen-containing groups can be associated with the lower oxygen content in the distillation residue. Thus, the results are in good agreement with the results of the elemental composition analysis.

Possible Application of the Distillates. The application of stabilized bio-oil distillates has not been so far widely investigated due to the common effort of researchers to obtain directly final products (hydrocarbon-based biofuels) by the bio-oil hydrotreatment under severe reaction conditions.[20,21,27,36] However, the physicochemical properties of hydrotreated liquid products may not fulfill the conventional fuels standards. Hence, the upgraded product integration into a refinery still needs to be further explored. Coprocessing of mild hydrodeoxygenated bio-oil with vacuum gas oil (VGO) in FCC has been reviewed by Zacher et al.[54] Fogassy et al.[55] reported that catalytic cracking of a mixture of VGO with mildly deoxygenated bio-oil resulted in gasoline and LCO yields comparable with catalytic cracking of VGO alone. However, yields of gaseous products and coke were higher. The hydrogenated bio-oils typically have a very broad distillation range, and thus, their coprocessing with a suitable middle distillate fraction will result in products having a broad distillation range. These will have to be fractionated into narrower fractions to be applicable as automotive fuels.

Despite the complex nature of the hydrotreated bio-oil, the product can be distilled with regards to crude-oil refinery and market needs in order to improve its applicability within the refinery fuel pools. Christensen et al.[38] also reported distillation ranges of hydrotreated bio-oil distillates, which were close to ours. Light gasoline was mainly composed of hydrocarbons and contained a small amount of carboxylic acids. Thus, light gasoline from bio-oil hydrotreatment is an appropriate fraction to be used directly in the gasoline pool.

On the other hand, heavy gasoline with a high content of water and carboxylic acids would require additional upgrading. However, this distillate can be a useful source of fine chemicals such as phenols or carboxylic acids. The diesel fraction contained a high concentration of phenolic compounds and carboxylic acids that would decrease the HHV and cause problems. Phenols from the diesel fraction can be additionally separated (e.g., by extraction) and used as a biochemicals, e.g., for bioresin manufacturing.[56] The diesel fraction could be also further hydrotreated separately or coprocessed with crude-oil middle distilled feedstock (e.g., LCO), to eliminate undesirable compounds in this fraction before being added to the diesel pool. It is worth noting that this could result in the formation of lighter deoxygenated products with boiling points in the range of heavy gasoline.

The distillation residue amounted to 31 wt % and corresponds to vacuum oil fractions. The main advantage of this fraction is its low oxygen content (in comparison with the distillates), low acidity, and high carbon content in the form of stigmastane structures and pyrolytic lignin. Thus, it could be coprocessed with crude-oil high-boiling-point distillates, e.g., vacuum distillates, in the hydrocracking process to produce lighter deoxygenated and dearomatized high-quality transportation fuels while avoiding extensive coke formation.

CONCLUSIONS

Several alumina- or silica-supported NiMo catalysts were prepared and tested in a single-stage fast pyrolysis bio-oil upgrading to obtain a hydrotreated product compatible with conventional hydrotreating processes. The assessment of these catalysts was performed in 80-h-long tests (340 °C, 4 MPa), and the catalysts were also benchmarked against two commercial catalysts. The silica-supported catalyst exhibited the worst performance among all tested catalysts both in HDS and HDO reactions. The three alumina-supported NiMo catalysts differed in their performance, despite having the same active NiMo phase loading and the same commercial alumina support used for their preparation. The differences were, thus, attributed to the preparation method and slightly different Ni/Mo atomic ratios. The catalyst prepared by coimpregnation outperformed the catalyst prepared by two-step impregnation procedures, and its overall performance was close to that of one of the commercial catalysts tested. Surprisingly, the other commercial catalyst showed the poorest performance among the alumina-based catalysts even though it has the best HDS

Downloaded from pubs.acs.org/ascecg/article-pdf/8/40/15149/6712707/acssuschemeng.0c03896.pdf by UNIV CHEMISTRY & TECHNOLOGY PRAGUE user on 26 October 2026

https://dx.doi.org/10.1021/acssuschemeng.0c03896
ACS Sustainable Chem. Eng. 2020, 8, 15149−15167

results. This demonstrates that the HDS activity of a catalyst is not a suitable indicator of its prospective performance in HDO of bio-oils.

The product properties deteriorated during 80 h on stream for all tested catalysts and reflected the loss of catalyst activity with the TOS due to their gradual deactivation. Although the changes are rather complex, a simple method based on principal component analysis of the FTIR spectra of the product was to monitor these changes. It could be further developed to provide real time data on the changes of the catalyst performance that, in turn, could be used for an adjustment of operating conditions to maintain constant product quality. One of the hydrotreated products was distilled to afford standard refinery fractions, i.e., naphtha (for gasoline production), middle distillate (for diesel fuel production), and atmospheric residue (for fuel oil production or as a feedstock of secondary upgrading processes, such as catalytic cracking or hydrocracking). This allowed more detailed identification of different types of oxygenates and their distribution among the different distillation cuts, which may be used when optimizing coprocessing parameters of these fractions with their petroleum-derived counterparts.

■ ASSOCIATED CONTENT

Supporting Information

The Supporting Information is available free of charge at https://pubs.acs.org/doi/10.1021/acssuschemeng.0c03896.

Additional information about catalyst preparation, description of principle component analysis and products analysis, selected properties, and composition of hydrotreatment products, and GC-MS composition of stabilized bio-oil distillates (PDF)

■ AUTHOR INFORMATION

Corresponding Author

Bogdan Shumeiko − *Department of Petroleum Technology and Alternative Fuels, University of Chemistry and Technology Prague, 166 28 Prague 6, Czech Republic;* orcid.org/0000-0003-1090-8971; Phone: +420220444238; Email: Bogdan.Shumeiko@vscht.cz

Authors

Miloš Auersvald − *Department of Petroleum Technology and Alternative Fuels, University of Chemistry and Technology Prague, 166 28 Prague 6, Czech Republic;* orcid.org/0000-0002-2449-6173

Petr Straka − *Department of Petroleum Technology and Alternative Fuels, University of Chemistry and Technology Prague, 166 28 Prague 6, Czech Republic*

Pavel Šimáček − *Department of Petroleum Technology and Alternative Fuels, University of Chemistry and Technology Prague, 166 28 Prague 6, Czech Republic*

Dan Vrtiška − *Department of Petroleum Technology and Alternative Fuels, University of Chemistry and Technology Prague, 166 28 Prague 6, Czech Republic*

David Kubička − *Department of Petroleum Technology and Alternative Fuels, University of Chemistry and Technology Prague, 166 28 Prague 6, Czech Republic;* orcid.org/0000-0003-2996-7824

Complete contact information is available at: https://pubs.acs.org/10.1021/acssuschemeng.0c03896

Notes

The authors declare no competing financial interest.

■ ACKNOWLEDGMENTS

The results were obtained in the BioMates project. This project has received funding from the European Union's Horizon 2020 research and innovation program under grant agreement No. 727463. The publication reflects only the authors' views; the Commission and its responsible executive agency INEA are not responsible for any use that may be made of the information it contains.

■ REFERENCES

(1) Schulzke, T.; Conrad, S.; Westermeyer, J. Ablative Flash Pyrolysis of Straw - Conversion Process and Valorization Options for Solid and Liquid Products.

(2) Mohan, D.; Pittman, C. U., Jr.; Steele, P. H. Pyrolysis of wood/biomass for bio-oil: a critical review. *Energy Fuels* **2006**, *20* (3), 848−889.

(3) Bridgwater, A. V. Review of fast pyrolysis of biomass and product upgrading. *Biomass Bioenergy* **2012**, *38*, 68−94.

(4) Auersvald, M.; Shumeiko, B.; Stas, M.; Kubicka, D.; Chudoba, J.; Simacek, P. Quantitative Study of Straw Bio-oil Hydrodeoxygenation over a Sulfided NiMo Catalyst. *ACS Sustainable Chem. Eng.* **2019**, *7* (7), 7080−7093.

(5) Gollakota, A. R.; Reddy, M.; Subramanyam, M. D.; Kishore, N. A review on the upgradation techniques of pyrolysis oil. *Renewable Sustainable Energy Rev.* **2016**, *58*, 1543−1568.

(6) Czernik, S.; Bridgwater, A. Overview of applications of biomass fast pyrolysis oil. *Energy Fuels* **2004**, *18* (2), 590−598.

(7) Auersvald, M.; Shumeiko, B.; Vrtiska, D.; Straka, P.; Stas, M.; Simacek, P.; Blazek, J.; Kubicka, D. Hydrotreatment of straw bio-oil from ablative fast pyrolysis to produce suitable refinery intermediates. *Fuel* **2019**, *238*, 98−110.

(8) Furimsky, E. Catalytic hydrodeoxygenation. *Appl. Catal., A* **2000**, *199* (2), 147−190.

(9) Elkasabi, Y.; Mullen, C. A.; Boateng, A. A.; Pighinelli, A. L. M. T. Hydrodeoxygenation of fast-pyrolysis bio-oils from various feedstocks using carbon supported catalysts. *Fuel Process. Technol.* **2014**, *123*, 11−18.

(10) Wildschut, J.; Mahfud, F. H.; Venderbosch, R. H.; Heeres, H. J. Hydrotreatment of Fast Pyrolysis Oil Using Heterogeneous Noble-Metal Catalyst. *Ind. Eng. Chem. Res.* **2009**, *48* (23), 10324−10334.

(11) Gholizadeh, M.; Gunawan, R.; Hu, X.; Kadarwati, S.; Westerhof, R.; Chaiwat, W.; Hasan, M. M.; Li, C.-Z. Importance of hydrogen and bio-oil inlet temperature during the hydrotreatment of bio-oil. *Fuel Process. Technol.* **2016**, *150*, 132−140.

(12) Laurent, E.; Delmon, B. Influence of Water in the Deactivation of a Sulfided NiMo/y-AI203 Catalyst during Hydrodeoxygenation. *J. Catal.* **1994**, *146*, 281−291.

(13) Rodríguez-Aguado, E.; Infantes-Molina, A.; Ballesteros-Plata, D.; Cecilia, J.; Barroso-Martín, I.; Rodríguez-Castellón, E. Ni and Fe mixed phosphides catalysts for O-removal of a bio-oil model molecule from lignocellulosic biomass. *Molecular Catalysis* **2017**, *437*, 130−139.

(14) Wildschut, J. *Pyrolysis Oil Upgrading to Transportation Fuels by Catalytic Hydrotreatment*. Dissertation, Rijksuniversiteit Groningen, 2009; pp 1−190, 978-90-367-4112-5.

(15) Mortensen, P. M.; Grunwaldt, J. D.; Jensen, P. A.; Knudsen, K. G.; Jensen, A. D. A review of catalytic upgrading of bio-oil to engine fuels. *Appl. Catal., A* **2011**, *407* (1−2), 1−19.

(16) Weisser, O.; Landa, S. *Sulphide catalysts, their properties and applications*; Elsevier: 2013; pp 11−506, 1483147614, DOI: 10.1016/C2013-0-02565-0.

(17) Horáček, J.; Kubička, D. Bio-oil hydrotreating over conventional CoMo & NiMo catalysts: The role of reaction conditions and additives. *Fuel* **2017**, *198*, 49−57.

(18) Priharto, N.; Ronsse, F.; Prins, W.; Hita, I.; Deuss, P. J.; Heeres, H. J. Hydrotreatment of pyrolysis liquids derived from second-

Downloaded from pubs.acs.org/ascecg/article-pdf/8/40/15149/6712707/acssuschemeng.0c03896.pdf by UNIV CHEMISTRY & TECHNOLOGY PRAGUE user on 26 October 2026

generation bioethanol production residues over NiMo and CoMo catalysts. *Biomass Bioenergy* **2019**, *126*, 84−93.
(19) He, Z.; Wang, X. Hydrodeoxygenation of model compounds and catalytic systems for pyrolysis bio-oils upgrading. *Catal. Sustainable Energy* **2012**, *1*, 28−52.
(20) Elliott, D. C.; Hart, T. R.; Neuenschwander, G. G.; Rotness, L. J.; Olarte, M. V.; Zacher, A. H.; Solantausta, Y. Catalytic Hydroprocessing of Fast Pyrolysis Bio-oil from Pine Sawdust. *Energy Fuels* **2012**, *26* (6), 3891−3896.
(21) Gholizadeh, M.; Gunawan, R.; Hu, X.; de Miguel Mercader, F.; Westerhof, R.; Chaitwat, W.; Hasan, M. M.; Mourant, D.; Li, C.-Z. Effects of temperature on the hydrotreatment behaviour of pyrolysis bio-oil and coke formation in a continuous hydrotreatment reactor. *Fuel Process. Technol.* **2016**, *148*, 175−183.
(22) Kadarwati, S.; Hu, X.; Gunawan, R.; Westerhof, R.; Gholizadeh, M.; Hasan, M. D. M.; Li, C.-Z. Coke formation during the hydrotreatment of bio-oil using NiMo and CoMo catalysts. *Fuel Process. Technol.* **2017**, *155*, 261−268.
(23) Zacher, A. H.; Elliott, D. C.; Olarte, M. V.; Wang, H.; Jones, S. B.; Meyer, P. A. Technology advancements in hydroprocessing of bio-oils. *Biomass Bioenergy* **2019**, *125*, 151−168.
(24) French, R. J.; Stunkel, J.; Black, S.; Myers, M.; Yung, M. M.; Iisa, K. Evaluate Impact of Catalyst Type on Oil Yield and Hydrogen Consumption from Mild Hydrotreating. *Energy Fuels* **2014**, *28* (5), 3086−3095.
(25) Ardiyanti, A.; Gutierrez, A.; Honkela, M.; Krause, A.; Heeres, H. J. A. C. A. G. Hydrotreatment of woodbased pyrolysis oil using zirconia-supported mono-and bimetallic (Pt, Pd, Rh) catalysts. *Appl. Catal., A* **2011**, *407* (1−2), 56−66.
(26) Kim, S.; Kwon, E. E.; Kim, Y. T.; Jung, S.; Kim, H. J.; Huber, G. W.; Lee, J. Recent advances in hydrodeoxygenation of biomass-derived oxygenates over heterogeneous catalysts. *Green Chem.* **2019**, *21* (14), 3715−3743.
(27) Huber, G. W.; Iborra, S.; Corma, A. Synthesis of transportation fuels from biomass: chemistry, catalysts, and engineering. *Chem. Rev.* **2006**, *106* (9), 4044−4098.
(28) Han, Y.; Gholizadeh, M.; Tran, C.-C.; Kaliaguine, S.; Li, C.-Z.; Olarte, M.; Garcia-Perez, M. J. F. P. T. *Fuel Process. Technol.* **2019**, *195*, 106140.
(29) Wan, H.; Chaudhari, R. V.; Subramaniam, B. J. E. fuels, Aqueous phase hydrogenation of acetic acid and its promotional effect on p-cresol hydrodeoxygenation. *Energy Fuels* **2013**, *27* (1), 487−493.
(30) Wang, W.; Yang, Y.; Luo, H.; Peng, H.; Wang, F. J. I.; Research, e. c. Effect of La on Ni−W−B Amorphous Catalysts in Hydrodeoxygenation of Phenol. *Ind. Eng. Chem. Res.* **2011**, *50* (19), 10936−10942.
(31) Zhao, C.; He, J.; Lemonidou, A. A.; Li, X.; Lercher, J. A. J. J. o. C. Aqueous-phase hydrodeoxygenation of bio-derived phenols to cycloalkanes. *J. Catal.* **2011**, *280* (1), 8−16.
(32) Zhao, C.; Kou, Y.; Lemonidou, A. A.; Li, X.; Lercher, J. A. J. C. C. Hydrodeoxygenation of bio-derived phenols to hydrocarbons using RANEY Ni and Nafion/SiO 2 catalysts. *Chem. Commun.* **2010**, *46* (3), 412−414.
(33) Saidi, M.; Samimi, F.; Karimipourfard, D.; Nimmanwudipong, T.; Gates, B. C.; Rahimpour, M. R. Upgrading of lignin-derived bio-oils by catalytic hydrodeoxygenation. *Energy Environ. Sci.* **2014**, *7* (1), 103−129.
(34) Viljava, T.-R.; Komulainen, R.; Krause, A.; Today, C. Effect of H2S on the stability of CoMo/Al2O3 catalysts during hydrodeoxygenation. *Catal. Today* **2000**, *60* (1−2), 83−92.
(35) Wang, W.; Zhu, G.; Li, L.; Tan, S.; Wu, K.; Zhang, X.; Yang, Y. J. F. Facile hydrothermal synthesis of flower-like Co−Mo−S catalysts and their high activities in the hydrodeoxygenation of p-cresol and hydrodesulfurization of benzothiophene. *Fuel* **2016**, *174*, 1−8.
(36) Routray, K.; Barnett, K. J.; Huber, G. W. Hydrodeoxygenation of pyrolysis oils. *Energy Technology* **2017**, *5* (1), 80−93.
(37) Olarte, M. V.; Zacher, A. H.; Padmaperuma, A. B.; Burton, S. D.; Job, H. M.; Lemmon, T. L.; Swita, M. S.; Rotness, L. J.; Neuenschwander, G. N.; Frye, J. G. Stabilization of softwood-derived pyrolysis oils for continuous bio-oil hydroprocessing. *Top. Catal.* **2016**, *59* (1), 55−64.
(38) Christensen, E. D.; Chupka, G. M.; Luecke, J.; Smurthwaite, T.; Alleman, T. L.; Iisa, K.; Franz, J. A.; Elliott, D. C.; McCormick, R. L. Analysis of Oxygenated Compounds in Hydrotreated Biomass Fast Pyrolysis Oil Distillate Fractions. *Energy Fuels* **2011**, *25* (11), 5462−5471.
(39) Christensen, E.; Ferrell, J.; Olarte, M. V.; Padmaperuma, A. B.; Lemmon, T. *Acid number determination of pyrolysis bio-oils using potentiometric titration*; Report No. NREL/TP-5100-65890; US Department of Energy: Washington, DC, 2016; p 17,. nrel.gov/docs/fy16osti/65890.pdf (accessed 2020-09-24).
(40) Shafaghat, H.; Rezaei, P. S.; Daud, W. M. A. W. Catalytic hydrodeoxygenation of simulated phenolic bio-oil to cycloalkanes and aromatic hydrocarbons over bifunctional metal/acid catalysts of Ni/HBeta, Fe/HBeta and NiFe/HBeta. *J. Ind. Eng. Chem.* **2016**, *35*, 268−276.
(41) Mortensen, P. M.; Grunwaldt, J.-D.; Jensen, P. A.; Jensen, A. D. J. A. C. Screening of catalysts for hydrodeoxygenation of phenol as a model compound for bio-oil. *ACS Catal.* **2013**, *3* (8), 1774−1785.
(42) Zhao, C.; Kou, Y.; Lemonidou, A. A.; Li, X.; Lercher, J. A. Highly Selective Catalytic Conversion of Phenolic Bio-Oil to Alkanes. *Angew. Chem., Int. Ed.* **2009**, *48* (22), 3987−3990.
(43) Nimmanwudipong, T.; Runnebaum, R. C.; Block, D. E.; Gates, B. C. Catalytic reactions of guaiacol: reaction network and evidence of oxygen removal in reactions with hydrogen. *Catal. Lett.* **2011**, *141* (6), 779−783.
(44) Wan, H.; Chaudhari, R. V.; Subramaniam, B. Catalytic hydroprocessing of p-cresol: metal, solvent and mass-transfer effects. *Top. Catal.* **2012**, *55* (3−4), 129−139.
(45) Wildschut, J.; Melian-Cabrera, I.; Heeres, H. Catalyst studies on the hydrotreatment of fast pyrolysis oil. *Appl. Catal., B* **2010**, *99* (1−2), 298−306.
(46) Yoosuk, B.; Tumnantong, D.; Prasassarakich, P. Amorphous unsupported Ni-Mo sulfide prepared by one step hydrothermal method for phenol hydrodeoxygenation. *Fuel* **2012**, *91* (1), 246−252.
(47) Zhao, H.; Li, D.; Bui, P.; Oyama, S. Hydrodeoxygenation of guaiacol as model compound for pyrolysis oil on transition metal phosphide hydroprocessing catalysts. *Appl. Catal., A* **2011**, *391* (1−2), 305−310.
(48) Andreev, A. A.; Kafedjiysky, V. J.; Edreva-Kardjieva, R. M. Active forms for water-gas shift reaction on NiMo-sulfide catalysts. *Appl. Catal., A* **1999**, *179* (1−2), 223−228.
(49) Wang, H.; Lian, Y.; Zhang, Q.; Li, Q.; Fang, W.; Yang, Y. MgO-Al2O3 mixed oxides-supported Co-Mo-based catalysts for high-temperature water-gas shift reaction. *Catal. Lett.* **2008**, *126* (1−2), 100−105.
(50) Valle, B.; Aramburu, B.; Olazar, M.; Bilbao, J.; Gayubo, A. G. J. F. Steam reforming of raw bio-oil over Ni/La2O3-αAl2O3: influence of temperature on product yields and catalyst deactivation. *Fuel* **2018**, *216*, 463−474.
(51) Montes, M.; Genet, M.; Hodnett, B.; Stone, W.; Delmon, B. X-Ray Photoelectron Spectroscopy of Sulfur Containing Ni/SiO2 Catalysts. *Bull. Soc. Chim. Belg.* **1986**, *95* (1), 1−12.
(52) Yoshimura, Y.; Yokokawa, H.; Sato, T.; Shimada, H.; Matsubayashi, N.; Nishijima, A. J. A. c. Temperature-programmed oxidation of sulfided nickel—molybdate/alumina catalysts Change of composition and structure of active metals. *Appl. Catal.* **1991**, *73* (1), 39−53.
(53) Patil, S. K.; Heltzel, J.; Lund, C. R. J. E. Fuels, Comparison of structural features of humins formed catalytically from glucose, fructose, and 5-hydroxymethylfurfuraldehyde. *Energy Fuels* **2012**, *26* (8), 5281−5293.
(54) Zacher, A. H.; Olarte, M. V.; Santosa, D. M.; Elliott, D. C.; Jones, S. B. A review and perspective of recent bio-oil hydrotreating research. *Green Chem.* **2014**, *16* (2), 491−515.
(55) Fogassy, G.; Thegarid, N.; Toussaint, G.; van Veen, A. C.; Schuurman, Y.; Mirodatos, C. Biomass derived feedstock co-

Downloaded from pubs.acs.org/ascecg/article-pdf/8/40/15149/6712170/acssuschemeng.0c03896.pdf by UNIV CHEMISTRY & TECHNOLOGY PRAGUE user on 26 October 2026

https://dx.doi.org/10.1021/acssuschemeng.0c03896
ACS Sustainable Chem. Eng. 2020, 8, 15149−15167

processing with vacuum gas oil for second-generation fuel production in FCC units. *Appl. Catal., B* **2010**, *96* (3−4), 476−485.
(56) Choi, G.-G.; Oh, S.-J.; Lee, S.-J.; Kim, J.-S. Production of bio-based phenolic resin and activated carbon from bio-oil and biochar derived from fast pyrolysis of palm kernel shells. *Bioresour. Technol.* **2015**, *178*, 99−107.

Downloaded from pubs.acs.org/ascecg/article-pdf/8/40/15149/6712707/acssuschemeng.0c03896.pdf by UNIV CHEMISTRY & TECHNOLOGY PRAGUE user on 26 October 2026

https://dx.doi.org/10.1021/acssuschemeng.0c03896
ACS Sustainable Chem. Eng. 2020, 8, 15149−15167